We thank the reviewer for taking the time to review this manuscript and the insightful comments. The reviewer comments are reproduced below in ***bold, italicized font***. Our responses are shown in regular font. Changes to the text are indicated as underlined text for insertions or are ~~crossed out~~ for deletions.

Anonymous Referee #1
Received and published: 16 October 2018
This paper presented a LED based cavity enhanced absorption spectroscopy at 470-540 nm. Different with previous CEAS instruments. The CEAS moved the window to cyan region (470-540 nm) and measure Rayleigh scattering cross-sections of several pure gases. This part is fundamental and very meaningful to the dataset. The authors applied the instrument to measure NO2 and I2 simultaneously. The measurement of ambient NO2 by CEAS was compared with CRDs and presented the feasibility. With respect to the I2 measurement by CEAS, which has been reported in the neighbor or the same wavelength region (e.g., Vaughan et al., 2008; Bahrini et al., 2018). Although the detecting capacity is not well improved compared with previous works, this work provides a possible way to measurement ambient I2. The following comments should be addressed before the consideration of publishing in AMT.

Major comments:
1. Section 3.3, it's interesting that using the saturated water vapor absorption to derive the effective optical absorption path determination. Are the authors make sure the water vapor was saturated by measured the RH? The sample flow of the water vapor gas keep the same with the ambient sampling flow or not (1.5-2.5 slpm). The authors should provide more details of the d0 determination, such as the convolution of effective water vapor cross section.

We thank the reviewer for having inquired about the use of water vapor in the determination of the effective absorption path and convolution of the water vapor cross-section. In response to the concerns raised, we have re-investigated the effective absorption path.

The setup used to generate gas streams saturated with water was the same as described in section 2.3.1 of (Woodward-Massey et al., 2014). In the earlier experiments, we had monitored the relative humidity (RH) using a commercial probe (VWR) and found the gas streams to be saturated. In hindsight, we agree with the reviewer that we should have monitored the RH in the experiments described in this manuscript as well, which we had not. One concern is that evaporative cooling of the liquid water reservoir could have lowered (and led to drifts in) the RH output of the source. Further, we did not observe condensation within the connecting tubing, and, again in hindsight, conclude that gas stream was likely not saturated. Another concern is that the water absorption lines in the cyan are narrower than the spectral resolution of our CEAS, such that the convolution (which has been added to Figure 1) could potentially have introduced a bias. Finally, the RH experiment was conducted at a flow rate of 1.0 slpm; at this low flow rate, R_L differs from that at a higher flow rate (see below).

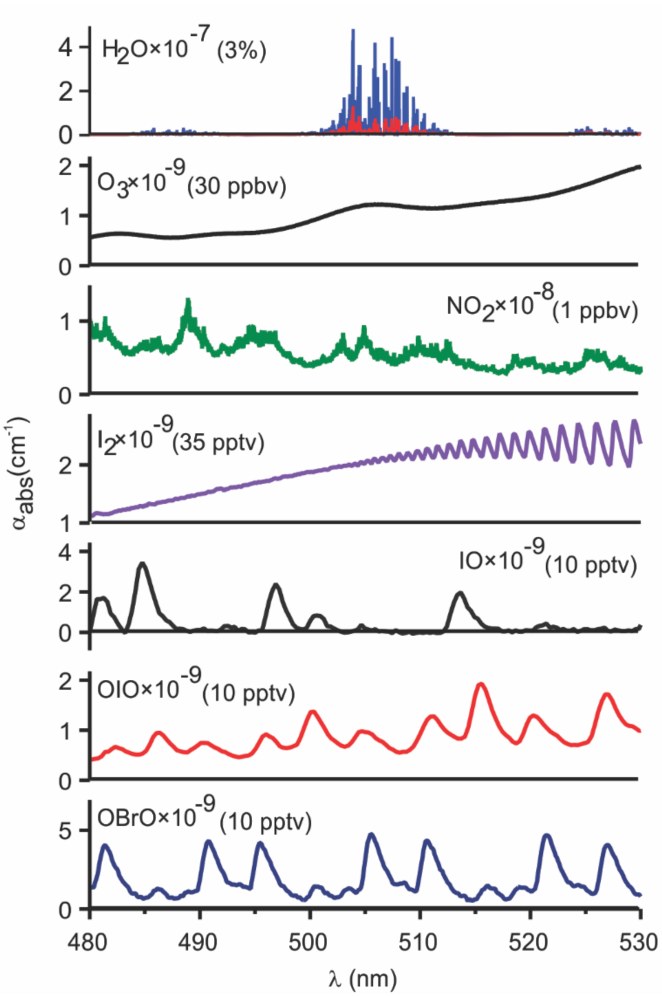

Figure 1. Absorption coefficients for atmospheric absorbers in the cyan region at typical tropospheric ~~abundances~~ mixing ratios (stated in brackets after each species). Absorption cross-sections were downloaded from the Max-Planck Institute for Chemistry's web site located at http://www.uv-vis-spectral-atlas-mainz.org and are based on the following: H_2O (Coheur et al., 2002), O_3 (Burkholder and Talukdar, 1994), NO_2 (Voigt et al., 2002), I_2 (Spietz et al., 2006), IO, OIO (Spietz et al., 2005), and OBrO (Knight et al., 2000). The literature cross-sections for H_2O (shown in blue) were convolved with the resolution of the IBBCEAS (shown in red). The absorption cross-section of O_4 is shown in Figure S4.

Because of the above concerns, we re-measured d_0 (i.e., R_L) for our sample cell. Since the work described in this manuscript, the IBBCEAS has been equipped with a new LED and mirrors optimal for the 350 - 390 nm wavelength region, where the O_2-O_2 collision pair has two absorption peaks near 361 and 380 nm. With this setup, we sampled pure molecular oxygen and calculated R_L from (a) the ratio of expected O_4 (calculated from known cross-sections and O_2 number density) divided by the ratio of O_4 observed and (b) by the turning the purge flows on and off (Duan et al., 2018). We used the recently reported cross-sections by (Thalman and Volkamer, 2013) with an accuracy of ±4.2% (1σ).

At a sample flow rate of ~2.0 slpm and purge flow rate of 0.1 slpm, and cell pressure of 870 hPa, we observed an R_L value (calculated using method (a)) of 1.28±0.05 (1σ precision stated) with an accuracy of ±5%. Consistent values were observed by method (b) ~20 min after the mirror purge flow had been turned off. We repeated this experiment sampling a constant concentration of NO_2 and obtained consistent results. This R_L value is smaller than calculated from the ratio of the inter-mirror distance *d* to the distance between the inlet and outlet of the sample flow (~1.39), which suggests that sampled air partially mixes into the purge volume.

Duan et al. (2018) reported a flow dependent R_L in their setup. Suspecting similar behaviour in our instrument, we measured R_L at a volumetric flow rate of up to 11 liters per minute (mass flow rate of ~4.4 slpm and a pressure of ~424 hPa), similar to conditions at which the instrument was operated during ORCA. We used method (a) to calculate R_L, since turning the purge flow of (method (b)) causes substantial pressure changes, and alternated sampling zero air and oxygen. At the larger flow rate, R_L was 1.20±0.07 (1σ precision).

On the basis of the above, we have rewritten section 3.3 as follows:
"When sampling ambient air, k~~K~~nowledge of the path length over which sampled air is present (d_0) and the associated correction factor R_L is essential ~~in experiments involving resonant optical cavities especially~~ for accurate IBBCEAS measurements when ~~purging~~ purge gases are used to maintain clean mirrors as in this work. ~~If the mirror reflectivity *R* is known, d_0 can be determined by measuring the extinction of a known amount of a strongly absorbing, non-reactive gas with known absorption cross-section, which is sampled through the inlet port. Combining Eq. (1) and Eq. (2) and rearranging gives an expression for d_0:~~

~~$$d_0 = \frac{\delta I(\lambda)}{\sigma N}\left(1 - R(\lambda) + d\alpha_{Ray}(\lambda)\right) \qquad (7)$$~~

~~Here, $\delta I(\lambda) = [I_0(\lambda) - I(\lambda)]/I(\lambda)$. In this work, we used water vapour and the absorption cross-section of H_2O from (Coheur et al., 2002) to determine $R_L = d/d_0$. A saturated gas stream of water vapour was generated by bubbling air through a water reservoir at a temperature of 298 K and pressure of 0.88 atm. Using Eq. (4), d_0 was found to be 73.2±0.7 cm, in agreement with the physical dimension (~73 cm) of the CEAS sample path. With d = 102.0 cm, this gives R_L = 1.39±0.01~~. The effective cavity length, d_0, was determined by sampling pure oxygen and monitoring the O_2 dimer (Duan et al., 2018). This experiment was performed in the 350 - 390 nm wavelength region using highly reflective mirrors and an LED (Thorlabs M365LP1) suitable for this wavelength region, though in principle it could have been performed in the cyan region as well since both spectral regions contain O_4 absorption lines. Following Duan et al. (2018), d_0 is given by

$$d_0 = d \times \frac{[O_2]_{on}}{[O_2]_{off}} \qquad (7)$$

where $[O_2]_{on}$ and $[O_2]_{off}$ are the $[O_2]$ retrieved using cross-sections by (Thalman and Volkamer, 2013) with or without the purge flows. Consistent results were obtained when a constant mixing ratio of NO_2 was sampled (and purge flows were turned on and off) and from the ratio of expected absorption by O_4 (calculated from the square of the number density of O_2 and the O_4 cross-section) relative to the observed O_4 absorption, though the latter may be less accurate as the absorption changes non-linearly in the region where purge and sample gases mix and requires accurate knowledge of mirror reflectivity.
At a sample flow rate of 2.0 slpm, a purge flow rate of 0.1 slpm, and a cell pressure of 870 hPa, we determined $R_L = d/d_0$ = 1.28±0.05 (1σ precision stated) with an accuracy of ±5%. This R_L value is smaller than calculated from the ratio of the inter-mirror distance d to the distance between the inlet and outlet of the sample flow (~1.39), which suggests that sampled air partially mixes into the purge volume. At a volumetric flow rate of 11 liters per minute as deployed during ORCA, we observed R_L = 1.20±0.07 (1σ precision)."

The results in section 4.1 are unaffected by this change, since the entire cell was filled with sample gases.

After remeasuring R_L, we discovered that it had not been correctly applied to the IBBCEAS data shown in Figures 5-8 and the results in sections 4.2 and 4.3; this has now been corrected. The following changes were made to the text:

Section 4.2.1 line 372:
"An NO_2 mixing ratio of (11.6 ± 0.4) ppbv was retrieved."
was changed to
"An NO_2 mixing ratio of (11.6 ± 0.4) ppbv was retrieved, corresponding to an ambient air mixing ratio of (13.9±1.0) ppbv when R_L is factored in."

Line 383: "Shown in Figure 7a is a scatter plot of all of the NO_x calibration data. This plot shows a linear relationship with a slope of 0.923±0.009, an intercept of 0.18±0.09 ppbv, and r^2 = 0.975. The slope of the line in Figure 7a reveals 7.7% difference in measurement of the calibration standard."
was changed to
"Shown in Figure 7a is a scatter plot of all of the NO_x calibration data. This plot shows a linear relationship with a

slope of 1.11±0.01, an intercept of 0.2±0.1 ppbv, and r^2 = 0.975. The slope of the line in Figure 7a reveals an 11% systematic difference in the measurement of the calibration standard."

Line 388: "The scatter plot of CEAS and CRDS NO_2 data (Figures 7b and 7c) suggest that the CRDS data were systematically higher than the CEAS data, by 15% when sampling ambient air (Figure 7c). When data are filtered by removing all CEAS points below a factor of three times the standard deviation of a blank measurement for 60 s (~1 ppbv; see Sect. 4.3), the slope of the scatter plot, when forced through an intercept of zero, is 0.98±0.01 (r^2 = 0.70)." was changed to

"For ambient air data collected on 18-19 Jul 2015, the scatter plot of IBBCEAS and CRDS NO_2 data (Figure 7b) has the same slope (1.12±0.02) as that shown in Figure 7a, while the scatter plot of the entire campaign has a slope of 1.02±0.01 (Figure 7C). When data are filtered by removing all IBBCEAS points below a factor of three times the standard deviation of a blank measurement for 60 s (~1 ppbv; see Sect. 4.3), the slope of the scatter plot, when forced through an intercept of zero, is 1.18±0.01 (r^2 = 0.70), suggesting that the IBBCEAS instrument is biased high."

We modified section 4.3 (Accuracy and limits of detection) as follows:

"The accuracy of the IBBCEAS NO_2 measurement is influenced by uncertainties in the absorption cross-section of NO_2 (±3%) (Voigt et al., 2002), fit errors ±(3 – 5%~~)~~, which can be reduced to ±(2 – 4)% by smoothing), scattering cross-sections, i.e., mirror reflectivity (±2.5%) (see Sect. 3.2 and 4.1), R_L (±5%; Sect. 3.3), and ~~calibration~~ errors in the mass flow controller reading (±1%), sample cell pressure readout (±0.5%), and temperature measurement (±0.7%). The total uncertainty, expressed as the square root of the individual errors summed in quadrature, is ±(~~5.5 – 7.6~~7 – 9)%. Not included in this estimate are errors arising from interpolation of infrequent mirror reflectivity and R_L determinations in the field."

In the subsequent text starting with "The limits of detection..." on line 414 and in the S.I. we have multiplied all values by the appropriate factor of R_L. This section now reads:

"The limits of detection (LOD) were assessed through Allan deviation analyses (Werle et al., 1993). For NO_2 sampled at a flow of 1.5 slpm and cell pressure of ~~668 Torr~~890 hPa, the Allan deviation was ±~~278~~ 360 pptv for 10 s data, ~~105~~ ±135 pptv for 60 s data, ~~49 pptv~~ and ±63 pptv for 5 min data averages (Figure 8a). At the higher sample flow of 5 slpm and reduced cell pressure of ~~350 Torr~~466 hPa used during the ORCA campaign, the ~~Allen~~ Allan deviation was ±~~137~~ 164 pptv for 334 s data (Figure S8).

For I_2 in laboratory-generated samples ~~under optimal conditions~~, typical 1σ fit errors ~~(when integrated over~~for 60 s~~)~~ averaged data were ±~~5.8~~7 pptv ~~for 21~~when 21 pptv I_2 were sampled and ±~~7~~ 9 pptv ~~for~~ when ~~350~~ 544 pptv I_2 were sampled (Figure S6). The accuracy ~~for~~ of I_2 data is, in principle, of similar magnitude to that of the NO_2 data, except that it also depends on knowledge of inlet transmission efficiency, which was not assessed in this work~~was (5.4 – 6.4)%, with main contribution from error in the high-resolution absorption cross-section of I_2 (Spietz et al., 2006)~~. The Allan deviation plot in Figure 8b demonstrates 1σ measurement precisions for I_2 of ±~~38~~ 49 pptv for 60 s and ±~~16~~ 22 pptv for 5 min averaged data. During ORCA, the 1σ precisions were ±~~100~~ 120 pptv for 60 s and ±~~50~~ 60 pptv for 5 min data, respectively.

For OIO, the Allan deviation analysis gives 1σ measurement precisions of ±~~4.6~~5.7 pptv for 60 s and ±~~1.8~~2.3 pptv for 5 min averaged data (Figure S9) in the laboratory. "

Finally, the following was inserted in the discussion section:

"An important parameter in any IBBCEAS measurement is the effective cavity length. Duan et al. recently summarized past practices in its determination and found that these practices vary considerably between groups (Duan et al., 2018). In this work, the necessary correction (R_L = 1.28 at 2.0 slpm sample flow rate) differed substantially from the physical dimension of the cell (1.39), underlining its importance for accurate measurements. However, it is unclear to what extent R_L varies between molecules which will need to be investigated. To improve the accuracy of future measurements, we will deploy more frequent zeroing (than during ORCA) and verify R_L periodically, for example by periodic sampling of molecular oxygen and measuring O_4 concentration."

2. The scatting cross section of N2 (Peck and Khanna, (1966)) was used in the calculation of reflectivity, but not included in the following intercomparison in figure 4(b), the author should clarify it.
Our apologies - the cross-section of Peck and Khanna (1966) had been mislabeled, which has been corrected.

3. Noticed that the cyan region was affected by the strong narrow absorption of water vapor (Bahrini et al., 2018). Here the author used a "new" zero that include the same water vapor concentration to avoid the interference (mentioned that in line 231). I think it's a good way to avoid the water vapor absorption problem, but the zero spectrum should be carried out more frequently in ambient condition and the reason why dynamic zero carried out should be addressed clearly in the text.
We agree that the zero determination should have been carried out more frequently when acquiring ambient air data. We added the following in section 3.8 on line 273: "Zero air was generated using a custom-built zero air generation system (Odame-Ankrah, 2015), which delivered air at ambient relative humidity that was free of trace gases such as NO_2, NO, I_2, or O_3. This approach minimized absorption by H_2O from the extinction spectra which can create artifacts (Bahrini et al., 2018)."

We also added the following to the discussion:
"An important parameter in any IBBCEAS measurement is the effective cavity length. Duan et al. recently summarized past practices in its determination and found that these practices vary considerably between groups (Duan et al., 2018). In this work, the necessary correction (R_L = 1.28 at 2.0 slpm sample flow rate) differed substantially from the physical dimension of the cell (1.39), underlining its importance for accurate measurements. However, it is unclear to what extent R_L varies between molecules (it is possibly larger for molecules with short lifetimes such as the IO radical) which will need to be investigated. To improve measurement accuracy in future measurements, we will deploy more frequent zeroing and verify R_L periodically, for example by periodic sampling of molecular oxygen."

4. Line 407, it's hard to make sure the wall loss of I2 in the inlet tube by just taking a look at the time series. The statement should be more conserve or just simply deleted as the author did not carry out more lab experiments to quantify the loss.
We agree with the reviewer that the inlet transmission of iodine species will need to be investigated more thoroughly in the future. On the other hand, the fast rise and fall times (which are shorter than the time resolution of our measurement) suggest the absence of inlet issues; our opinion is based experience with other reactive gases (e.g., the nitrate radical, and molecular chlorine), and is worthwhile stating.
We have modified the sentence in question from "The square-wave response and quick rise and fall times suggest the absence of inlet transmission losses." to "While the transmission of iodine through inlets was not systematically investigated in this work, t~~T~~he square-wave response and quick rise and fall times suggest the absence of inlet transmission losses."

Specific comments:
1. Keywords are not necessary in AMT.
They have been removed.

2. Line 48, please make up the reference. (2010) as well as in line 220.
We have added the author names to the references as requested by the reviewer.

3. Line 370 and line 394 , “an example” should be change to “a spectrum retrieve example” or “a spectrum fitting example”

We have changed the text in question from "An example NO_2 CEAS measurement is shown on Figure 5a." to "An example of a spectral retrieval for NO_2 in ambient air ~~CEAS measurement~~ is shown on Figure 5a." and from "Figure 5b shows an example of an I_2 measurement." to "Figure 5b shows an example ~~of an~~retrieval for I_2 ~~measurement~~."

4. Line 392, R2 is 0.70.

This has been corrected.

5. Line 422, is “60 s and ±50 pptv for 5 minutes, respectively.”

Fixed.

6. The residual plots in Figure 5 and Figure S5 should be united to the style in Figure S3.

We have updated Figures 5 and S5 as requested and have taken the opportunity to update the depiction of the polynomial, which was displayed incorrectly.

7. I suggest the authors put the figure S7 in the main text though the ambient I2 below the instrument LOD.

Since the ambient air mixing ratio of I_2 was below our detection limit, we prefer to leave the Figure in the S.I.

Literature cited:

Bahrini, C., Grégoire, A.-C., Obada, D., Mun, C., and Fittschen, C.: Incoherent broad-band cavity enhanced absorption spectroscopy for sensitive and rapid molecular iodine detection in the presence of aerosols and water vapour, Optics & Laser Technology, 108, 466-479, 10.1016/j.optlastec.2018.06.050, 2018.

Burkholder, J. B., and Talukdar, R. K.: Temperature-Dependence of the Ozone Absorption-Spectrum over the Wavelength Range 410 to 760 nm, Geophys. Res. Lett., 21, 581-584, 10.1029/93GL02311, 1994.

Coheur, P. F., Fally, S., Carleer, M., Clerbaux, C., Colin, R., Jenouvrier, A., Merienne, M. F., Hermans, C., and Vandaele, A. C.: New water vapor line parameters in the 26000-13000 cm^{-1} region, J. Quant. Spectrosc. Radiat. Transf., 74, 493-510, 10.1016/S0022-4073(01)00269-2, 2002.

Duan, J., Qin, M., Ouyang, B., Fang, W., Li, X., Lu, K., Tang, K., Liang, S., Meng, F., Hu, Z., Xie, P., Liu, W., and Häsler, R.: Development of an incoherent broadband cavity-enhanced absorption spectrometer for in situ measurements of HONO and NO_2, Atmos. Meas. Tech., 11, 4531-4543, 10.5194/amt-11-4531-2018, 2018.

Knight, G., Ravishankara, A. R., and Burkholder, J. B.: Laboratory studies of OBrO, J. Phys. Chem. A, 104, 11121-11125, 10.1021/jp002226u, 2000.

Odame-Ankrah, C. A.: Improved detection instrument for nitrogen oxide species, Ph.D., Chemistry, University of Calgary, http://hdl.handle.net/11023/2006, 10.5072/PRISM/26475, Calgary, 2015.

Spietz, P., Gómez Martín, J. C., and Burrows, J. P.: Spectroscopic studies of the I_2/O_3 photochemistry: Part 2. Improved spectra of iodine oxides and analysis of the IO absorption spectrum, J. Photochem. Photobiol. A, 176, 50-67, 10.1016/j.jphotochem.2005.08.023, 2005.

Spietz, P., Gómez Martín, J., and Burrows, J. P.: Effects of column density on I_2 spectroscopy and a determination ofI_2 absorption cross section at 500 nm, Atmos. Chem. Phys., 6, 2177-2191, 10.5194/acp-6-2177-2006, 2006.

Thalman, R., and Volkamer, R.: Temperature dependent absorption cross-sections of O_2-O_2 collision pairs between 340 and 630 nm and at atmospherically relevant pressure, Phys. Chem. Chem. Phys., 15, 15371-15381, 10.1039/c3cp50968k, 2013.

Voigt, S., Orphal, J., and Burrows, J. P.: The temperature and pressure dependence of the absorption cross-sections of NO_2 in the 250-800 nm region measured by Fourier-transform spectroscopy, Journal Of Photochemistry And Photobiology A-Chemistry, 149, 1-7, 10.1016/S1010-6030(01)00650-5, 2002.

Woodward-Massey, R., Taha, Y. M., Moussa, S. G., and Osthoff, H. D.: Comparison of negative-ion proton-transfer with iodide ion chemical ionization mass spectrometry for quantification of isocyanic acid in ambient air, Atmos. Environm., 98, 693-703, 10.1016/j.atmosenv.2014.09.014, 2014.

We thank the reviewer for taking the time to review this manuscript and the insightful comments. The reviewer comments are reproduced below in ***bold, italicized font***. Our responses are shown in regular font. Changes to the text are indicated as underlined text for insertions or are ~~crossed out~~ for deletions.

Anonymous Referee #2

Received and published: 19 October 2018

This discussion paper reports on the development of a broadband cavity-enhanced absorption spectrometer, using incoherent light from a light emitting diode (LED) in the cyan region of the spectrum; i.e. between 470 and 540 nm. The performance of the instrument has been evaluated and characterized in the laboratory as well as in the field concerning the detection of NO2 and I2. It was further utilized to measure Rayleigh scattering cross-sections of several gases for calibration and validation purposes.

This is a well written and thoroughly prepared manuscript with good attention to detail, however, the approach to trace gas detection using incoherent broadband cavity enhanced absorption spectroscopy (IBBCEAS) is not new. In fact there is a continually growing number of IBBCEAS instruments for field, chamber, and laboratory studies and the merit of this manuscript is predominantly in the discussion of the usefulness of the cyan region for NO2 and I2 detection, as well as the independent measurement and assessment of scattering cross-sections of several gases (O2, N2, air, Ar, CO2 and CH4) which are relevant for calibration purposes and remote sensing applications, and add to the overall accuracy and knowledge of data in the literature on optical losses of the corresponding gases. Publication in Atmospheric Measurement Techniques is thus warranted in my opinion,

We thank the reviewer for this kind assessment.

subject to addressing the following aspects which caught my attention during reviewing the discussion paper:

P1 In Line 12 (Abstract) the authors introduce the acronym (CEAS) as cavity-enhanced absorption spectrometer, however, in Line 27 (Introduction) CEAS stands for cavity-enhanced absorption spectroscopy. Generally the term CEAS is used in the context of spectroscopy (just like cavity-ring down spectroscopy, CRDS). In the manuscript the authors refer to their instruments as "the CEAS", or "the CRDS", but still also use the other definition synonymously. For clarity and conformity with previous literature using CEAS as a "spectroscopy acronym". I recommend using the term "CEAS instrument" or "CRDS instrument". Moreover, in order to distinguish the experimental methodology from a laser-based approach (coherent) light, the term "IBBCEAS instrument" (see above) in this context is unambiguous.

We agree with the above argument and have made the suggested changes throughout the text.

Line 35: The authors refer to retrieval techniques that are analogous to those used in differential optical absorption spectroscopy (DOAS). Standard DOAS retrieval cannot be applied to the measured spectra, as only an effective pathlength is known in CEAS if the mirror reflectivity is known; thus the mirror reflectivity is key to the spectral analysis. The authors may want to rephrase this statement.

The statement has been rephrased as follows: "The output spectrum is integrated yielding extinction spectra from which mixing ratios are retrieved using ~~techniques analogous to those used in differential optical absorption spectroscopy (DOAS) (Platt and Stutz, 2008)~~known absorption spectra and knowledge of the mirror reflectivity and effective optical absorption path (Meinen et al., 2010)."

P2 Line 3: In the context of NO3 the authors may want to cite (Venables et al., 2006; Varma et al., 2008) which are not listed among the references.

We have added citations to (Venables et al., 2006) and (Varma et al., 2009) as suggested by the reviewer.

In line 4 other papers on I2 detection (Dixneuf et al., 2009; Ball et al., (2010); Nitschke et al., (2011); Bahrini et al., (2018)) may be mentioned, one of which is already in the reference list.

We have added citations to (Ball et al., 2010; Dixneuf et al., 2009; Bahrini et al., 2018) but have chosen not cite the Nitschke paper here because the methodology is described in the earlier paper by (Dixneuf et al., 2009). We cite Nitschke et al. (2011) on line 68.

P4 The authors may want to use σ_n instead of σ (introduced in Eq. (5)) to indicate "n-based" cross-sections.

Done.

Line 107 & 110: "resonant optical cavity" -> "optical cavity"

Fixed.

Line 116: Backing pressure stated in psi with conversion to Pa given. Later on all pressures are given in torr. This should probably be uniform. Since this is a European journal probably psi and torr should be avoided and pressures should be stated in mbar or Pa.

We have replaced the pressure unit Torr with SI unit (hPa) throughout the text.

Line 124: The authors may want to state the LED's optical output power here.

We have added the information requested and removed the phrase "to achieve a manufacturer quoted optical minimum output power of ~400 mW" from line 162 as it is now redundant.

P5 Line 138: discrete

Fixed.

Line 141: yielded an approximately Gaussian profile with -> yielded approximately Gaussian profiles of the atomic Hg emission lines with

Fixed.

Line 142: degraded -> lower

Fixed.

Line 146: net instrument weight -> net weight of the instrument

Fixed.

Line 163: asymmetric Lorentzian shape? What is meant by that? Just refer to Figure 3.

We have removed word Lorentzian.

P6 Line 172: “and d is in units of cm.” Either delete this (recommended) or also state that α is in units of cm^{-1}.

We have removed the phrase as recommended by the reviewer.

Line 196: an uncertainty of +/0.1 % in pressure appears rather small given the fact that this is a flow cell experiment.

On line 180, we state that "the gases were continuously injected through the purge ports until all other sample cell constituents were displaced through the open inlet port"; typical flow rates were ~100 sccm. The inner diameter of the sample cell tube is 1.59 cm and relatively large; hence, we wouldn't expect much uncertainty due to a relatively modest flow.

No changes were made.

Line 196: an uncertainty of +/0.1 % in light intensity appears somewhat optimistic when looking at Figure S10.

Since the relative standard deviation of the data shown in Figure S10 is indeed with in ±0.1%, no changes were made to the manuscript in response to this comment.

P7 Line 219: “Convolving the NO2 ... effectively degraded the high...”. The spectrum is not really “degraded”, it is simply corrected for a different resolution. This sentence can be deleted in my opinion.

We have changed the sentence "Convolving the NO_2 reference spectrum effectively degraded the high-resolution spectrum but was required for the least-squares analysis." to "A ~~C~~convolved~~ing~~ ~~the~~ NO_2 reference spectrum ~~effectively degraded the high-resolution spectrum but~~ was ~~required~~ used for the least-squares analysis."

Line 219-221: The authors state that the literature cross-sections of I2 and OIO were not convolved as the spectrometers resolution was higher than the resolution at which the literature spectra were measured. I do not quite follow this. The reference spectra for the fit should still be adapted to the resolution of the spectrometer used since otherwise the cross-sections do not match. What was the resolution of the literature spectra used?

We inserted "at a resolution of 0.59 nm ".

Also: (2005; 2006) -> (Spietz et al. 2006; 2005)

Fixed.

Line 224: “(relatively) low resolution CEAS instrument” -> “IBBCEAS instrument”

Fixed.

Line 233 & 234: If the water concentrations were significant they should have been included in the fit in any case and not just to minimize the residuals. However, fitting water spectra is generally difficult, since water absorption lines in the visible are genuinely spectrally narrow; in other words the resolution of the spectrometer may be small in comparison to the FWHM of water absorption features. In this case the absorption behavior is not in the Lambert-Beer regime and the H2O reference spectra used in the fit must be corrected for that fact (see Bitter et al. 2005; Varma et al., 2008). I am wondering whether the H2O mixing ratios obtained in those fits were indeed

meaningful. They do not seem to be stated in the manuscript. If H2O mixing ratios from the fit are not meaningful, then including H2O simply introduces one more degree of freedom to the fit and therefore smaller residuals can be achieved, but this is physically not justified. The H2O cross-sections in the cyan region are small in any case and might be discarded depending on the humidity during the campaign? Also see Bahrini et al., (2018) where I2 was measured in the presence of water vapour – water was simply subtracted?!

We apologize for the confusion - the next sentence clearly states that water was included in the fit (we meant to say to that the contributions by water were small and often negligible). We agree with the reviewer that fitting to the high-resolution water spectrum in this wavelength region is challenging and derived mixing ratios will not be quantitative. We attempted to avoid this issue, either by using water-free gases (as was the case for the Rayleigh scattering cross-section measurements) or by attempting to have the same water concentration in both the zero and measurement spectra, such that water only minimally contributed to the optical extinction spectra.

We have changed the text on line 233 as follows:

"The "spectral shifting" setting in DOASIS was set to ±0.2 nm, and stretching was disallowed. ~~The contributions of water vapor to the optical extinction was neglected since the relative humidity of the air sampled during the background measurement was the same as during the measurement of NO_2 or I_2.~~

The same parameters were used to fit the data from the ORCA field campaign except that in an effort to minimize the fit residuals, the convoluted absorption cross-section of H_2O based on the high-resolution data by (Coheur et al., 2002) was also included in the fit. The contributions of water vapor to the optical extinction was ~~neglected~~small since the relative humidity of the air sampled during the background measurement was the same as during the measurement of NO_2 or I_2."

Line 235: What criteria determined the smoothing parameters that yielded better seemingly better results?

In general, fourth order polynomial Savitzky/Golay digital filtering routine is commonly applied in many areas of science (including chromatography and spectroscopy). In our work, we found smoothing using this readily available algorithm did improve the signal to noise ratio of our measurement. However, the digital filtering parameters (or alternate filtering algorithms) were not systemically explored, as this is outside the scope of this manuscript.

No changes were made to the manuscript.

P8 The pure gases for reflectivity and scattering cross-section measurements are not mentioned in section 3.7.

Apologies for this oversight.

In response to the reviewer's comment, we expanded a sentence in section 3.2: "To determine $R(\lambda)$ in this work, the cavity output intensity was recorded when the cell was filled with high purity N_2 (99.998%) or with He (99.998%) to atmospheric pressure (~890 hPa). In each case, the gases were delivered from a compressed gas cylinder (Praxair) and continuously injected through the purge ports until all other sample cell constituents were displaced through the open inlet port."

Further, we modified section 3.7:

"3.7 Generation and delivery of ~~calibration~~ gases
Figure 2b shows ... (i.e., wall thickness and length).
Ar, CO_2, CH_4, N_2, O_2, air and He were delivered from compressed gas cylinders (Praxair) in the same manner as described in section 3.2."

Molecular iodine is a very sticky molecule. Do the authors have any information on, or attempted to measure iodine losses in the inlet system (see also next comment).

P9 Line 270: Did the authors try to calibrate line losses concerning I2?

This was not attempted. We made the following change in section 4.2.2:

"Figure S7 shows a sample time series of I_2 mixing ratios during the ORCA campaign. Concentrations of I_2 (and of OIO, not shown) in ambient air were below the instrument's detection limits. At 22:30 UTC, I_2 from a diffusion source was added to the inlet. While the transmission of iodine through inlets was not systematically investigated in this work, ~~The~~ the square-wave response and quick rise and fall times suggest the absence of inlet transmission losses."

Line 271: in regular intervals -> at regular intervals

Fixed.

Line 286: "...coefficients)," insert comma

Fixed.

P11 Line 348 & 349:(1973) -> (Bideau-Mehu et al., 1973)(1977) -> (Shardanand and Rao, 1977) same in Line 352(2005) -> (Sneep and Ubachs, 2005)

Fixed.

P12 Line 372/373: "The residual spectrum is lacking structure, indicating ..." The residuals in Figure 5a show asymmetric residuals, which appear to have spikes that appear to "go negative", they are not balanced (log scale?). This is strange,

The residuals are as calculated by DOASIS. We note that there are both positive and negative spikes. The average ± 1 standard deviation are $(-0.02\pm5.05)\times10^{-9}$ cm^{-1} for the residual NO_2 spectrum (Fig. 5a) and $(-0.1\pm8.1)\times10^{-9}$ cm^{-1} for the residual I_2 spectrum (Fig. 5B), so they are not misbalanced. The slightly larger residual for the I_2 spectrum may have been a result of a tiny misalignment of the reference and observed spectra wavelength scales.

in particular since the same figure is shown in the supplemental material (Figure S3). Here the residuals appear more balanced. The authors may want to check this, as it seems the data are the same but the residuals differ. Moreover, part of Figure S3 appears redundant.

In Figure S3, we are comparing the results obtained when fitting spectra with a digital filter applied to the data and without. We reproduced the data in Figure 5a in Figure S3A, but on a different scale to facilitate this comparison. Since this is in the supplemental, we have chosen to not amend the manuscript in response to the reviewer's comment.

Line 375: The authors claim that there were up to 16 ppbv of NO2 in the standard gas mixture. In Figure 6a mostly 10 ppbv are observed (with one exception that is higher). Where does this information of the 16 ppbv come from?

This mixing ratio was determined by blue diode laser CRDS, as stated ("During the ORCA campaign, the inlet of the IBBCEAS instrument (and of the CRDS instrument, which sampled in parallel) was overflowed every 30 min with a standard gas mixture of ~20 ppbv NO_x containing up to 16 ppbv of NO_2 in zero air and with ~130 ppbv of NO added to ambient air."). No changes were made in response to this question.

The reason for overflowing the sample cell with two different mixtures is not clear to me.

This was done for reasons outside the scope of this paper, but since the reviewer asked: we also operated an N_2O_5 channel (heated inlet, 662 nm diode laser) of the main sample line; it is common practice to "zero" such a channel by titration with a high NO concentration. We had reasons to distrust the supplier's stated concentration of the more concentrated NO gas cylinder (for one, its certificate had expired), and opted to cross-calibrate with a more recently purchased calibration gas cylinder.

We added the following on line 278: "A PAN-GC (Tokarek et al., 2014), commercial NO/NO_y and O_3 instruments (Thermo 42i and 49i), as well as a 662 nm diode laser N_2O_5 channel (Osthoff et al., 2017) also sampled off this common inlet line, resulting in all instruments periodically sampling a variety of calibration gases."

Why did the authors chose the specific "format" (=measurement procedure) shown in Figure 6, to characterize the instument.

Please see our answer above.

The zeroing periods are not indicated in Figure 6.

This has been added.

Section 4.2.2. Only one figure on molecular iodine is shown in the main body of the text. All other figures on iodine are in the supplemental material (Figs. S5, S6, S7). This is too much information in the additional information section. At least one time series should be shown in the main paper in my opinion.

Since the ambient air mixing ratio of I_2 was below our detection limit, the time series are of marginal value to the reader. We hence prefer to leave the Figure displaying its time series in the S.I.

Line 398: How was the mixing ratio of I2, outflowing from the permeation chamber, established?

The stated iodine mixing ratios were from IBCCEAS retrievals (as no independent iodine measurement was on hand). In response to the reviewer's question, we have removed the following sentence "The smallest amount of I_2 that was produced without dilution of the permeation chamber output flow was ~21 pptv" from the manuscript.

P13 Line 423/424: The information on OIO measurements and the Allan deviation analysis for same appear very suddenly at this point in the paper (section 4.3). Measured OIO spectra are not shown or, if present in the I2 spectra, not mentioned. Formation of OIO is not discussed. OIO was insufficiently discussed prior to section 4.3 and the supplemental material also only shows Allan deviation plots, rather than measurement or evaluation procedure. The authors should say more about OIO detection in the paper.

The chemistry leading to formation of OIO is well documented in the literature (e.g., (Cox et al., 1999; Allan et al., 2001; Saiz-Lopez et al., 2006; Huang et al., 2010)) and outside the scope of this paper. In response to the reviewer's comments, we have changed the title of section 4.22 from "Molecular iodine" to "Iodine species (I_2 and OIO)" and have modified a sentence on line 405:

"Concentrations of I_2 (and of OIO, not shown) in ambient air were below the instrument's detection limits."

In the discussion, we already stated the following:

"The sensitivity for I_2 and OIO (~~16~~ 19 and ~~1.8~~2.1 pptv for 5 min averaged data under laboratory conditions) suffices for their quantification in environmental chamber studies (Dixneuf et al., 2009). Further, these LODs are below maximum I_2 and OIO abundances reported at Mace Head, Ireland, of 94 and 13 pptv (Bitter et al., 2005) and 61 and 9.2 pptv (Peters et al., 2005), respectively, but above the maximum I_2 level of 4 pptv reported in California (Finley and Saltzman, 2008). This implies that iodine species on the West coast of British Columbia, Canada, might have been detected if the instrument had been operated optimally."

We do not believe that further modifications are warranted.

P14 Line 455: refer to the last paragraph in the discussion on Page 15 rather than listing future system "upgrades" in brackets and "etc."

We have modified the paragraph in question as follows:

"The detection limit for NO_2 achieved under laboratory conditions in this work (49 pptv for 5 min data) is ~~compared~~ of similar magnitude as those by ~~to~~ instruments operated in other wavelength regions (Table 2). However, the CEAS measurement precision in this work was surpassed by the more mature blue diode CRDS, though future upgrades (~~e.g., more highly reflective mirrors, more sensitive spectrometer, etc.~~ see below) may improve the CEAS precision."

Line 465: Conclusions are drawn on OIO, but too little is said about OIO in the manuscript.

Please see answer to the comment re lines 423/424.

References

Suggested additions:

Ball et al. Atmos. Chem. Phys. 10, 6237-6254, (2010) now cited

Bahrini et al., Opt. Laser Techn. 108, 466-479, (2018) now cited

Nitschke et al. Planta 233, 737-748, (2011) now cited

Varma et al. Appl. Opt. 48, B159-B171, (2009) now cited

Venables et al. Env. Sci. Techn. 40, 6758-6763, (2006) now cited

P18 Include initials of Shardanand.

Unfortunately, we cannot since this author did not use a first name in any of his or her publications.

Figure 3: List pressures in the caption

Done.

Figure 4f: Holm -> Hohm

Done.

Figure 5a: Check data in the residual panel (see comments above, I think the data are logarithmic plotted on a linear axis)

Figure 5 was updated (partially in response to a comment by reviewer 1).

Figure 6: Please also indicate the time when zero air was flown into the cavity

Done.

Figure 7 (panel b and c). Units missing after intercept

added

P28 Include ref (King, 1923) in caption

added

Supplementary Material

Figure S5: Improve the caption, which is simply too short for what is shown in the figure. Is there an offset in the data shown in the uppermost panel? The colour code is unclear and the assignment of residuals also (coloured residuals are too congested). What is to be conveyed through the log and linear axes? Blue residuals in the middle panel are unclear. I think this figure needs attention.

We have modified Figure S5 as follows:

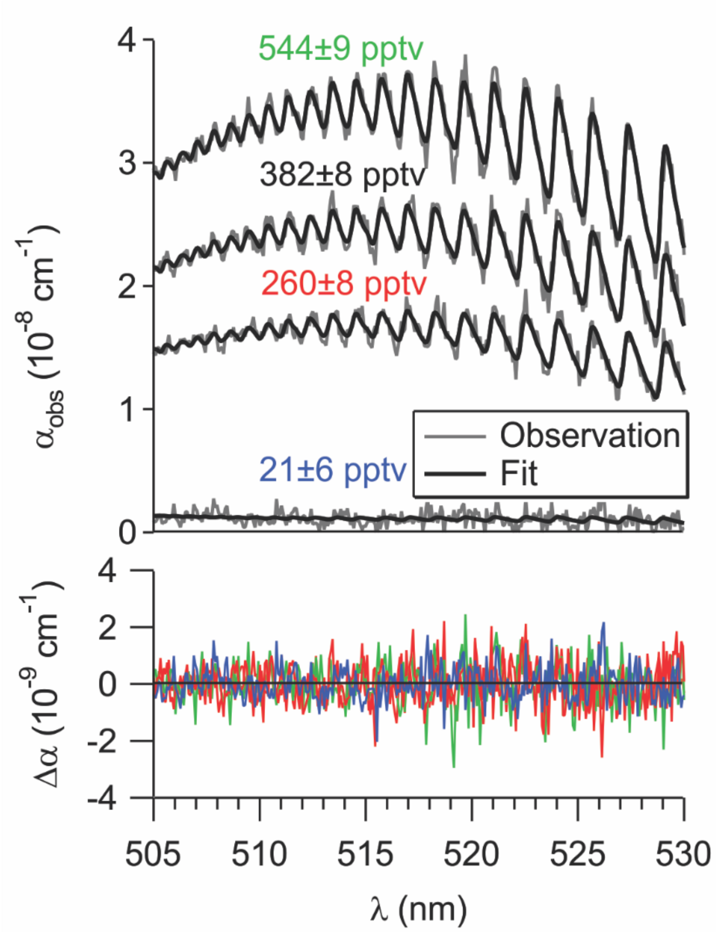

Figure S5 Examples of spectral fits of laboratory generated I_2 at different mixing ratios. The absorption cross-sections by Spietz et al. (2006) and a third-order polynomial were used. The bottom panel shows the fit residuals, colour-coded by the mixing ratio labels above.

In response to reviewer's comment, we have combined the top two panels and plotted the data on a linear scale. We thank the reviewer for noticing that the top three traces were offset; in fact, their mixing ratios were incorrectly stated, and this has now been corrected.

Figure S6: What is going on between 21:20 and 21:30? Is there zero air sampling?

We thank the reviewer for catching this error. Indeed, the instrument sampled zero air from 21:20 to 21:30. The figure now displays the zeroing periods correctly.

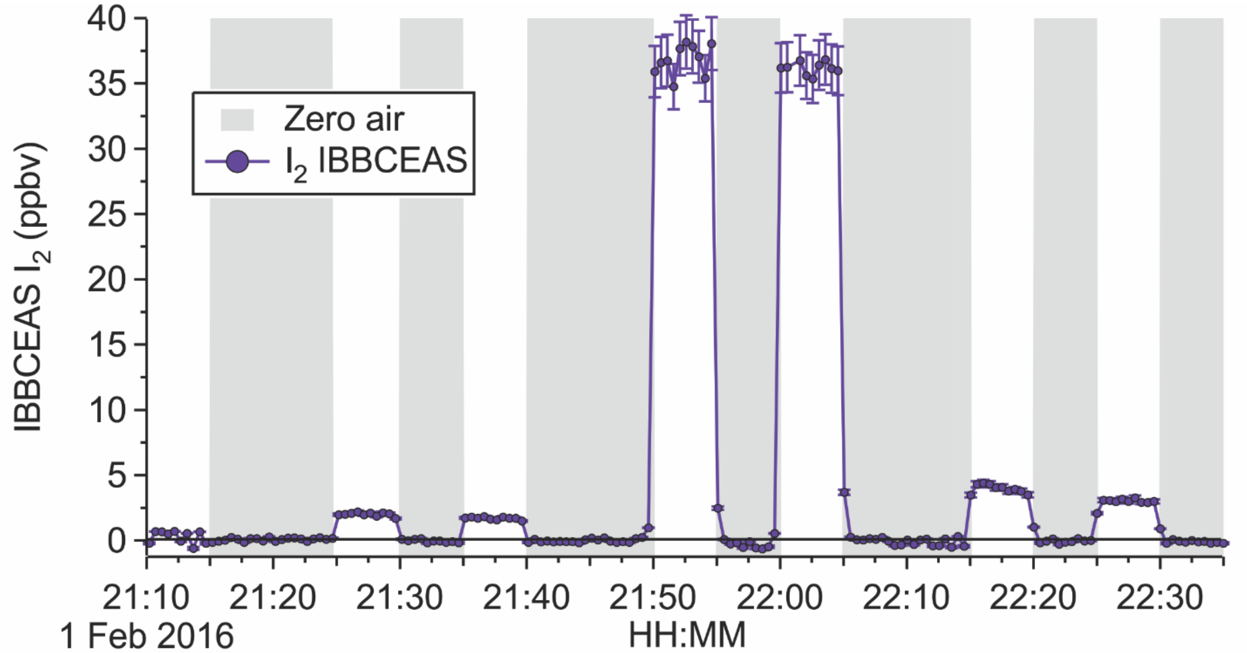

Figure S6 Time series of sample CEAS retrievals while sampling laboratory generated I_2. The grey underlay indicates times when the instrument sampled zero air. Iodine was delivered from four permeation tubes of different wall thickness, which were exchanged during the zeroing periods while the diffusion chamber output was bypassed.

Are there error bars on all data points? Are they too small to be seen except for during the two concentration maxima?

There are error bars on all data points, and there are indeed too small to be seen. No changes were made in response to this question.

Figure S8: In the left panel the minimum does not seem to have been reached. The same is true in Figure S9.

Figures S8 was combined with the top panel of Figure S9. The minimum was not reached as we are showing data for the longest zeroing period during ORCA, which lasted 15 min. The data are instructive insofar as they provide a contrast to the laboratory conditions. No changes were made in response to this comment, though the figures were modified to account for the R_L value.

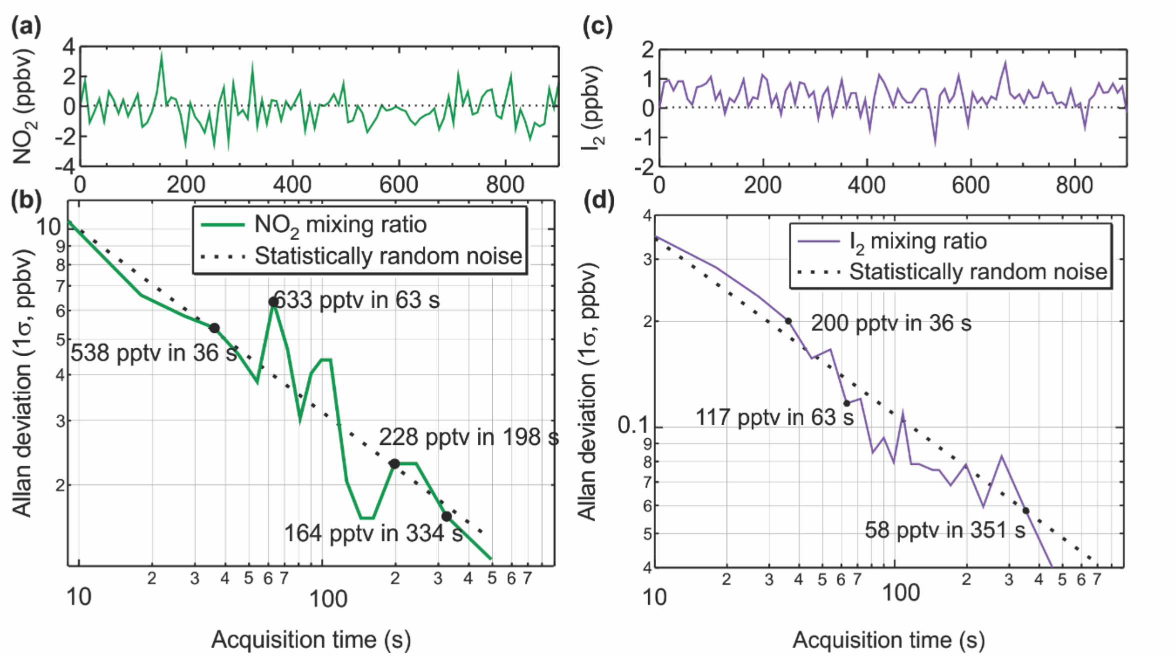

Figure S8 Data collected while the CEAS continuously sampled zero air during the ORCA campaign at a sample cell pressure of 467 hPa, flow rate of 5 slpm, and at a temperature 290 K. (**a**) Time series of NO_2 mixing ratios. (**b**) Allan deviation plot of the above data. (**c**) Time series of I_2 mixing ratios. (**d**) Allan deviation plot of the above data.

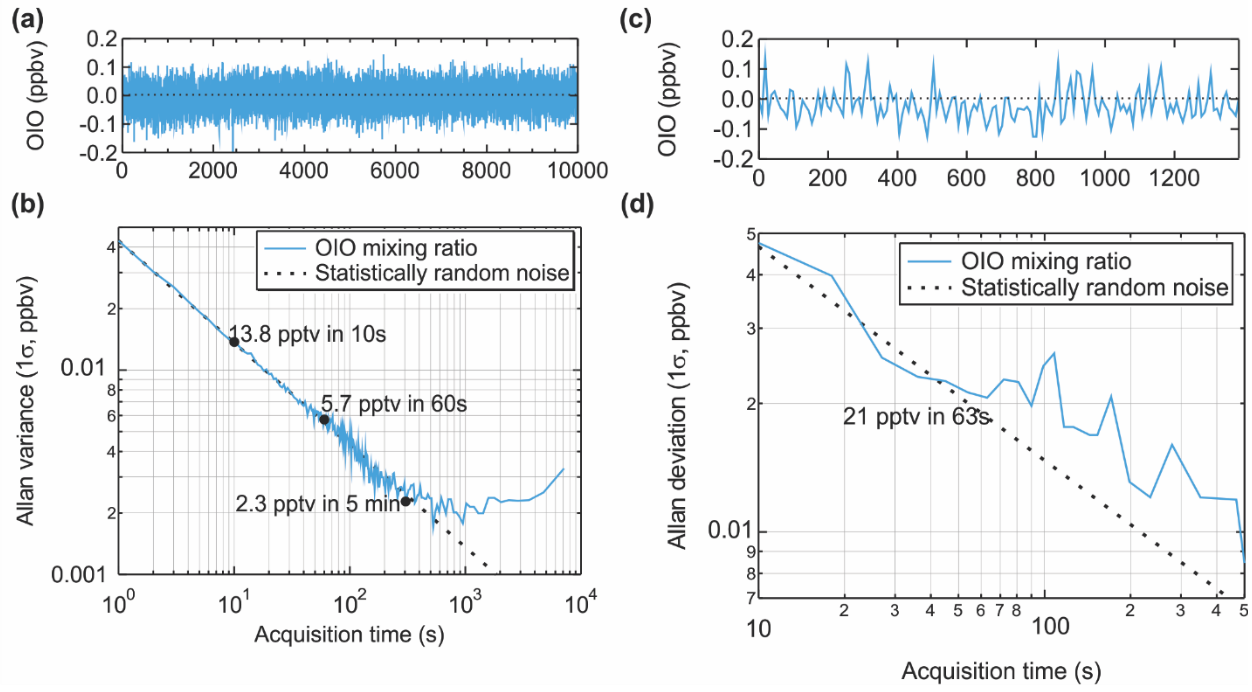

Figure S9 (left hand side) Data collected while the CEAS continuously sampled zero air in the laboratory at a sample cell pressure of 890 hPa, flow rate of 1.5 slpm, and at a temperature 298 K. (**a**) Time series of OIO mixing ratios. (**b**) Allan deviation plot of the above data. (right hand side) Data collected while the CEAS continuously sampled zero air during the ORCA campaign at a sample cell pressure of 467 hPa, flow rate of 5 slpm, and at a temperature 290 K. (**c**) Time series of OIO mixing ratios during ORCA. (**d**) Allan deviation plot of the above data.

Figure S9: More explanation on OIO is needed in my opinion.

Please see our answer for line 465 (pg 14) above.

Figure S10: CEAS emission profile for a cavity filled .... -> Intensity of light exiting a cavity filled with zero air. Three different wavelength regions within the emission spectrum of an LED (M505L3) driven at .... is shown.

We have modified the figure caption as suggested by the reviewer.

Literature cited

Allan, B. J., Plane, J. M. C., and McFiggans, G.: Observations of OIO in the remote marine boundary layer, Geophys. Res. Lett., 28, 1945-1948, 10.1029/2000GL012468, 2001.

Bahrini, C., Grégoire, A.-C., Obada, D., Mun, C., and Fittschen, C.: Incoherent broad-band cavity enhanced absorption spectroscopy for sensitive and rapid molecular iodine detection in the presence of aerosols and water vapour, Optics & Laser Technology, 108, 466-479, 10.1016/j.optlastec.2018.06.050, 2018.

Ball, S. M., Hollingsworth, A. M., Humbles, J., Leblanc, C., Potin, P., and McFiggans, G.: Spectroscopic studies of molecular iodine emitted into the gas phase by seaweed, Atmos. Chem. Phys., 10, 6237-6254, 10.5194/acp-10-6237-2010, 2010.

Cox, R. A., Bloss, W. J., Jones, R. L., and Rowley, D. M.: OIO and the atmospheric cycle of iodine, Geophys. Res. Lett., 26, 1857-1860, 10.1029/1999gl900439, 1999.

Dixneuf, S., Ruth, A. A., Vaughan, S., Varma, R. M., and Orphal, J.: The time dependence of molecular iodine emission from Laminaria digitata, Atmos. Chem. Phys., 9, 823-829, 10.5194/acp-9-823-2009, 2009.

Huang, R. J., Seitz, K., Buxmann, J., Pohler, D., Hornsby, K. E., Carpenter, L. J., Platt, U., and Hoffmann, T.: In situ measurements of molecular iodine in the marine boundary layer: the link to macroalgae and the implications for O_3, IO, OIO and NOx, Atmos. Chem. Phys., 10, 4823-4833, 10.5194/acp-10-4823-2010, 2010.

Osthoff, H. D., Odame-Ankrah, C. A., Taha, Y. M., Tokarek, T. W., Schiller, C. L., Haga, D., Jones, K., and Vingarzan, R.: Low levels of nitryl chloride at ground level: Nocturnal nitrogen oxides in the Lower Fraser Valley of British Columbia, Atmos. Chem. Phys., 18, 6293-6315, 10.5194/acp-18-6293-2018, 2017.

Saiz-Lopez, A., Shillito, J. A., Coe, H., and Plane, J. M. C.: Measurements and modelling of I_2, IO, OIO, BrO and NO_3 in the mid-latitude marine boundary layer, Atmos. Chem. Phys., 6, 1513-1528, 10.5194/acp-6-1513-2006, 2006.

Tokarek, T. W., Huo, J. A., Odame-Ankrah, C. A., Hammoud, D., Taha, Y. M., and Osthoff, H. D.: A gas chromatograph for quantification of peroxycarboxylic nitric anhydrides calibrated by thermal dissociation cavity ring-down spectroscopy, Atmos. Meas. Tech., 7, 3263-3283, 10.5194/amt-7-3263-2014, 2014.

Varma, R. M., Venables, D. S., Ruth, A. A., Heitmann, U., Schlosser, E., and Dixneuf, S.: Long optical cavities for open-path monitoring of atmospheric trace gases and aerosol extinction, Appl. Optics, 48, B159-B171, 10.1364/AO.48.00B159, 2009.

Venables, D. S., Gherman, T., Orphal, J., Wenger, J. C., and Ruth, A. A.: High sensitivity in situ monitoring of NO_3 in an atmospheric simulation chamber using incoherent broadband cavity-enhanced absorption spectroscopy, Environm. Sci. Technol., 40, 6758-6763, 10.1021/es061076j, 2006.

A broadband cavity-enhanced spectrometer for atmospheric trace gas measurements and Rayleigh scattering cross sections in the cyan region (470-540 nm)

Nick Jordan,[1] Connie Z. Ye,[1] Satyaki Ghosh,[1] Rebecca A. Washenfelder,[2] Steven S. Brown,[2] and Hans D. Osthoff[1]

[1] Department of Chemistry, University of Calgary, 2500 University Drive NW, Calgary, AB T2N 1N4, Canada

[2] Earth System Research Laboratory, National Oceanic and Atmospheric Administration, 325 Broadway, Boulder, CO 80303, USA

Correspondence: Hans D. Osthoff (hosthoff@ucalgary.ca)

Abstract. An incoherent broadband cavity-enhanced absorption spectrometer (IBBCEAS) instrument for quantification of atmospheric trace gases that absorb in the cyan region of the electromagnetic spectrum (470 to 540 nm), including NO_2 and I_2, is described. The instrument uses a light-emitting diode coupled to a 1 m optical cavity consisting of a pair of mirrors in stable resonator configuration. Transmitted light is monitored using a grating spectrometer and charge-coupled device array detector. The average mirror reflectivity was determined from the N_2/He and Ar/He ratios of scattering coefficients and was ~99.98% at its maximum, yielding an effective optical path length of 6.3 km. Cross-sections of N_2, O_2, air, Ar, CO_2, and CH_4 scattering and of O_4 absorption were measured and agree with literature values within the measurement uncertainty. Trace gas mixing ratios were retrieved using the spectral fitting software DOASIS from 480 to 535 nm. Under laboratory conditions, the 60 s, 1σ measurement precisions were ±~~105~~ 124 and ±~~38~~ 44 pptv for NO_2 and I_2, respectively. The IBBCEAS instrument sampled ambient air in Ucluelet, BC, in July 2015. IBBCEAS retrievals agreed with independent measurements of NO_2 by blue diode laser cavity ring-down spectroscopy ($r^2 = 0.975$), but ambient I_2 concentrations were below the detection limit.

~~**Keywords**: Cavity-enhanced spectroscopy, cyan region, Rayleigh scattering cross-sections, atmospheric trace gas measurements, nitrogen dioxide, iodine~~

1 Introduction

~~Broadband c~~Cavity-enhanced absorption spectroscopy (CEAS) has emerged in recent years as a sensitive technique for direct measurement of atmospheric trace gases (Fiedler et al., 2003; Gherman et al., 2008; Vaughan et al., 2008; Washenfelder et al., 2008; Schuster et al., 2009; Thalman and Volkamer, 2010; Hoch et al., 2014) and of aerosol optical extinction (Thalman and Volkamer, 2010; Bluvshtein et al., 2012; Washenfelder et al., 2013). Similar to other cavity-enhanced techniques (Gagliardi and Loock, 2014), CEAS owes its high sensitivity to highly reflective mirrors (reflectivity, $R > 99.9\%$) which yield long effective absorption path lengths. In CEAS, light generated from a high intensity broad-band light source (e.g., a Xe arc lamp) is transmitted through an optical cavity set up in a stable resonator configuration. The output spectrum is integrated yielding extinction spectra from which mixing ratios are retrieved using ~~techniques analogous to those used in differential optical absorption spectroscopy~~known absorption spectra and knowledge of the mirror reflectivity and effective optical absorption path ~~(DOAS) (Platt and Stutz, 2008)~~(Meinen et al., 2010). To date, CEAS ~~has~~ instruments have been used to quantify mixing ratios of many atmospherically important trace gases, including nitrogen dioxide (NO_2) (Langridge et al., 2008; Gherman et al., 2008; Triki et al., 2008; Thalman and Volkamer, 2010; Wu et al., 2014; Min et al., 2016; Varma et al., 2009), the nitrate radical (NO_3) (Langridge et al., 2008; Schuster et al., 2009; Venables et al., 2006; Varma et al., 2009), iodine (I_2) (Ball et al., 2010; Dixneuf et al., 2009; Bahrini et al., 2018), the iodine oxides IO and OIO (Vaughan et al., 2008), glyoxal (HCOHCO) (Washenfelder et al., 2008; Thalman and Volkamer, 2010; Coburn et al., 2014; Min et al., 2016), methyl glyoxal (CH_3COCHO) (Thalman and Volkamer, 2010; Thalman et al., 2015; Min et al., 2016), molecular bromine (Br_2), bromine monoxide (BrO) (Chen and Venables, 2011; Hoch et al., 2014), formaldehyde (Washenfelder et al., 2016), and nitrous acid (HONO) (Gherman et al., 2008; Wu et al., 2014; Min et al., 2016).

The accuracy of retrievals depends on knowledge of relevant absorption and scattering (i.e., Rayleigh) cross-sections (which both contribute to the optical extinction) and of the mirror reflectivity. Because of its high sensitivity, CEAS in turn has been utilized to measure these parameters. For example, Axson et al. and Kahan et al. recently reported the absorption cross-sections of O_3 and H_2O_2 (Axson et al., 2011; Kahan et al., 2012), and Thalman and Volkamer reported scattering cross-sections of N_2, O_2, Ar, and air (Thalman and Volkamer, 2010) for several wavelength intervals (345 – 390, 435 – 490, 515 – 545, 560 – 600, and 600 – 700 nm).

In spite of the large number of CEAS instruments that have been constructed, the mid-visible region has received relatively little attention to date, other than the pioneering study by Vaughan et al. (2008), even though the absorption maxima of several key atmospheric traces gases, such as NO_2 and the iodine species I_2, IO and OIO, are located in this wavelength interval (Figure 1). The study of iodine chemistry has been of considerable interest due to potential effects on the formation of new particles and atmospheric oxidising capacity through, for example, catalytic destruction of O_3, altering the partitioning of NO_x (= NO + NO_2) and HO_x (= HO + HO_2), or the activation of chlorine and bromine from sea salt aerosol in the marine and polar boundary layer, near salt lakes and volcanoes, and in the stratosphere (Saiz-Lopez et al., 2012). Prior laboratory measurements by Vaughan et al. used a 150 W Xenon arc lamp; such light sources tend to flicker, i.e., exhibit intensity fluctuations, which add noise to the absorption spectrum. For this and other reasons (such as compactness, heat generation, etc.), light-emitting diodes (LEDs) are now commonly used to generate broad-band radiation (Washenfelder et al., 2008; Min et al., 2016).

In this paper, we describe an LED-powered incoherent broadband cavity-enhanced absorption spectroscopy (~~broadband~~ IBBCEAS) instrument operated in the cyan region of the electromagnetic spectrum. We report laboratory measurements of scattering cross-sections for N_2, O_2, Ar, CO_2, CH_4 and air from 480 to 535 nm and demonstrate detection of NO_2 and I_2 in laboratory-generated air. The IBBCEAS instrument was operated during the Ozone-depleting Reactions in a Coastal Atmosphere (ORCA) field campaign, conducted July 8-31, 2015 at the Amphitrite Point Observatory (APO) in Ucluelet on the west coast of Vancouver Island, British Columbia (Tokarek et al., 2017). Kelp forests are present along this coast line (Watson and Estes, 2011), which are expected to emit I_2 (Dixneuf et al., 2009; Nitschke et al., 2015; Nitschke et al., 2011). Mixing ratios of NO_2 retrieved from the cyan IBBCEAS data are compared to those measured by a co-located blue diode laser cavity ring-down spectrometer. The potential of the instrument for quantification of iodine species in laboratory and field experiments is assessed.

2 Theory

2.1 Cavity-enhanced spectroscopy

The principle of broadband trace gas measurements by IBBCEAS has been described elsewhere (Fiedler et al., 2003; Washenfelder et al., 2008). Briefly, broadband radiation is continuously injected and trapped between a set of highly reflective mirrors forming a stable resonant cavity. The integrated cavity output intensity represents the combined extinction by the mirrors and the intra cavity medium. The absorption coefficient, $\alpha_{abs}(\lambda)$, is given in terms of the transmission signal through the cavity (Washenfelder et al., 2008) by Eq. (1):

$$\alpha_{abs}(\lambda) = R_L \left(\frac{1-R(\lambda)}{d} + \alpha_{Ray}(\lambda)\right)\left(\frac{I_0(\lambda)-I(\lambda)}{I(\lambda)}\right) \tag{1}$$

Here, R_L (see Sect. 3.3) is the ratio of the cell length ($d \approx 102$ cm) divided by the length occupied by the sample ($d_0 \approx$ ~~73~~ 82 cm - section 3.3), $R(\lambda)$ is the average wavelength dependent mirror reflectivity, d is the distance between the two reflective surfaces (i.e. the cavity length), $\alpha_{Ray}(\lambda)$ is the sum of all Rayleigh scattering sample constituents, $I_0(\lambda)$ is the intensity spectrum in the absence of absorbers in the cavity cell, and $I(\lambda)$ is the intensity spectrum measured in the presence of absorbers. When measurements are carried out in variable pressure environments (e.g., aircraft altitude change), an additional term ($\Delta\alpha_{Ray}(\lambda)$) is added to Eq. (1) to account for pressure fluctuations (Min et al., 2016). If multiple absorbers are present in the cavity, the absorption coefficient becomes the sum of all species expressed as in Eq. (2) (Washenfelder et al., 2008).

$$\alpha_{abs} = \sum_i^n \alpha_i(\lambda) = \sum_i^n N_i\, \sigma_i(\lambda, T, p) \tag{2}$$

Here, $\sigma_i(\lambda, T, p)$ is the wavelength, temperature, and pressure-dependent absorption cross-section, and N_i is the number density of the i^{th} absorbing gas.

2.3 Determination of Rayleigh scattering cross-sections

Cavity-enhanced spectroscopic techniques allow accurate and precise measurements of Rayleigh scattering cross-sections of pure gases over broad wavelength regions (Naus and Ubachs, 2000; Sneep and Ubachs, 2005; Axson et al., 2011; Kahan et al., 2012; Thalman et al., 2014). If the mirror reflectivity $R(\lambda)$ is known, the scattering cross-section of any gas can be determined by measuring its extinction and that of a reference gas (Thalman et al., 2014), e.g., for CO_2 and using He as a reference:

$$\alpha_{Ray}^{CO_2}(\lambda) = \left(\left(\frac{1-R(\lambda)}{d}\right)\left(1-\frac{I_{CO_2}(\lambda)}{I_{He}(\lambda)}\right) + \alpha_{Ray}^{He}(\lambda)\right)\left(\frac{I_{He}(\lambda)}{I_{CO_2}(\lambda)}\right) \tag{3}$$

Here, $\alpha_{Ray}(\lambda)$ is the optical extinction (in cm^{-1}) caused by the intra-cavity scattering medium. The scattering cross-sections are then calculated through division by the number density of the gas (N_{gas}), i.e.,

$$\sigma_{Ray}(\lambda) = \frac{\alpha_{Ray}(\lambda)}{N_{gas}} \tag{4}$$

Scattering cross-sections can be predicted if the refractive index, n, of a gas is known (Naus and Ubachs, 2000; Sneep and Ubachs, 2005), hereafter referred to as an "n-based" cross-section, σ_n:

$$\sigma_n \cancel{\sigma}(\nu) = \frac{24\pi^3\nu^4}{N^2}\left(\frac{n^2(\nu)-1}{n^2(\nu)+1}\right)^2 F_k(\nu) \tag{5}$$

Here, ν is the frequency in wavenumbers (cm^{-1}), $n(\nu)$ is the frequency dependent refractive index of the gas, and F_k is the King depolarization ratio which describes the effect of molecular anisotropy (King, 1923).

3 Experimental

3.1 Description of the IBBCEAS instrument

The IBBCEAS instrument consists of an LED light source, collimating optics, a high finesse ~~resonant~~ optical cavity, focusing optics, specialized fibre bundle, and a spectrograph equipped with a charge-coupled device (CCD) camera (Figure 2).

The ~~resonant~~ optical cavity consists of two dielectric-coated, plano-concave fused silica substrate mirrors (Advanced Thin Films, Boulder, CO, USA) with maximum reflectivity from 460 to 550 nm, 2.54 cm in diameter, 0.635 cm thickness, and 1 m radius of curvature. To span a broad wavelength range, the mirrors were coated with two highly reflective substrates, resulting in a double maximum in their reflectivity. The mirrors were mounted on both ends of a 102 cm long cell with a gas sampling region of ~73 cm and housed in a custom-built mount equipped with purge gas ports. A flow of 50 standard cubic centimeters per minute (sccm) of ultrapure air ("zero" grade, Praxair) set using 50 µm critical orifices (Lenox Laser, Glen Arm, MD, USA) and a gas regulator back pressure of ~~20 pounds per square inch (psi; 1 psi = 6.9~~138 kPa~~)~~ was directed to each mirror to protect the optical surfaces from contamination. The mirror mounts were attached to adjustable kinematic mounts (Newport U200-A, Irvine, CA, USA) each equipped with 3 set screws for mirror alignment. The gas sampling region was enclosed using 1.9 cm outer diameter (o.d.) and 1.59 cm inner diameter (i.d.) fluorinated ethylene propylene (FEP) Teflon™ tubing (Saint Gobain Plastics, Chemfluor series). The Teflon™ tube was held in place by a custom enclosure constructed from Aluminium. Gases entered and exited the sampling region through 1.9 cm o.d. perfluoroalkoxy alkane (PFA) Teflon™ fittings (Entegris Fluid Handling, Billerica, MA, USA).

The LED (Thorlabs M505L3, Newton, NJ, USA; 400 mW nominal output power) output was collimated into the cavity by a single f/0.8 aspheric condenser lens (Thorlabs ACL2520U-A). The cavity output was collected and focused by a 2.5 cm diameter f/1 lens through a non-polarizing quartz beam splitter (Thorlabs BS025) onto a 0.5 cm (diameter) f/4 fibre adapter that couples the radiation into a 2 m long 0.22 numerical aperture (NA) fibre bundle (Thorlabs BFL200HS02). The beam splitter has 90% transmission efficiency in the plane parallel to the cavity and 10% in the orthogonal plane and was used to direct the emission lines of a Hg(Ne) spectral calibration lamp (Newport Oriel 6032) towards the detector for calibration of the spectrometer wavelength scale and line width. The fibre bundle consists of 7 × 200 µm optical fibres arranged with circular and linear configurations on the input and output, respectively. The fibre bundle output was oriented linearly along the spectrograph entrance slit to optimize coupling of the cavity output similar to (Min et al., 2016; Washenfelder et al., 2016), and illuminated the full vertical dimension of the CCD. Spectra were acquired by a 150 cm focal length f/4 dual grating Czerny-Turner spectrograph (Princeton Instruments Acton SP2156, Trenton, NJ, USA) which back-illuminates a 16-bit 1340 × 100 pixel CCD array (Princeton Instruments, PIXIS 100B), mounted at the focal plane of the spectrograph and Peltier-cooled to -80 °~~o~~C to reduce thermal noise. The spectrograph was configured with a 1200 groove mm^{-1} grating blazed at 500 nm. This configuration along with the grating positioned at 500 nm central wavelength yielded spectral coverage from 446.9 to 563.2 nm spanning a total of 1340 ~~discreet~~ discrete wavelength points. The Acton SP2156 spectrograph shipped with a mechanical shutter, which was removed in lieu of software control of the integration time via LABVIEW™ (National Instruments, Austin TX, USA).

A fixed entrance slit width of 50 µm yielded ~~an~~ approximately Gaussian profiles of the atomic Hg emission lines with full-width at half maximum (FWHM) of (0.330±0.003) nm at 540.06 nm. Other spectral lines (e.g., 520.39 nm) showed slightly ~~degraded~~ lower resolution of roughly (0.360±0.016) nm (Figure S1). An integration time of 5-6 s saturated the CCD pixels 80–90% of their well depth near 500 nm.

All mechanical and optical components were mounted on an optical breadboard (Thorlabs MB2448) bolted onto aluminium structural rails (80/20, Columbia City, IN, USA). The net weight of the instrument ~~weight~~ including the breadboard and railing is < 90 kg and the overall power consumption below 300 W.

The IBBCEAS instrument samples air through a 47 mm diameter, circular, permeable polytetrafluoroethylene (PTFE) Teflon™ membrane filter with 1 µm pore size (Pall Teflon™ Series, Port Washington, NY, USA) housed in a PFA Teflon™ filter holder (Cole-Parmer R-06621-40) and through 0.635 cm outer diameter and 0.476 cm FEP Teflon™ tubing. The sample flow was set using a mass flow controller (MFC, MKS Instruments 100 B series, 15 standard litres per minute (slpm) capacity, Andover, MA, USA) connected to a diaphragm pump (KNF Neuberger UNO26.1.2ATP, Trenton, NJ, USA). The sample flow was in the range 1.5–2.5 slpm resulting in a sample residence time of 5.9–3.5 s. The gas temperature was measured using a K-type thermocouple (Omega, Laval, QC, Canada) attached to the aluminium sample cell enclosure. Pressure was measured using a pressure transducer (MKS Baratron capacitance manometer 722B) mounted on the exhaust portion of the IBBCEAS between the gas sample cell and the MFC.

The light source is a small footprint (1×1 mm) broadband LED (M505L3, Thorlabs) mounted on the end of a heat sink supplied by the manufacturer. We modified this assembly by mounting a Peltier module (CUI Inc. CP30238, Tualatin, Oregon, USA) between the LED and the heat sink for temperature control using a proportional–integral–derivative (PID) controller (Omega CNi3253) to 30.0±0.1 ºC. If not stabilized, the LED output red-shifted ~0.1 nm per °C temperature change. The LED was operated just below the maximum current of 1000 mA (3.3 W of electrical power) ~~to achieve a manufacturer quoted optical minimum output power of ~400 mW~~.

The LED output spectrum was characterized by an asymmetric ~~Lorentzian~~ shape, an emission maximum at 507.5 nm, and a peak width of 22.5 nm FWHM, and was a good match with the mirror reflectivity curve (Figure 3).

3.2 Determination of the mirror reflectivity

The response of the IBBCEAS instrument depends on $R(\lambda)$ and d_0 (Eq. (1)), which need to be accurately known. If an optical cavity is filled with a non-absorbing and inert gas, and aerosol are removed by filtering, the optical extinction is due to gas scattering only. In this case, $R(\lambda)$ can be derived from the extinction caused by two individual gases with known and different scattering cross-sections such as N_2 and He (Washenfelder et al., 2008):

$$R(\lambda) = 1 - d\,\frac{\alpha_{Ray}^{N_2}(\lambda)\frac{I_{N_2}(\lambda)}{I_{He}(\lambda)} - \alpha_{Ray}^{He}(\lambda)}{1 - \frac{I_{N_2}(\lambda)}{I_{He}(\lambda)}} \qquad (6)$$

Here, $I_X(\lambda)$and $\alpha_{Ray}^{X}(\lambda)$are the intensities and extinction coefficients of N_2 and He, respectively~~, and d is in units of cm~~. Other pairs (e.g., He and Ar) may be used as well. For this work, we chose scattering cross-sections from (Peck and Khanna, 1966) for N_2, (Cuthbertson and Cuthbertson, 1932) for He, and (Peck and Fisher, 1964) for Ar. Typically, combinations with He provide a higher signal-to-noise due to He having a much smaller scattering cross-section than other gases (Thalman et al., 2014). The above approach assumes that scattering and absorption within the optical cavity are small (Washenfelder et al., 2008) and neglects absorption and scattering due to the mirror substrate.

To determine $R(\lambda)$ in this work, the cavity output intensity was recorded when the cell was filled with high purity N_2 (99.998%) or with He (99.998%) to atmospheric pressure (~890 hPa). In each case, the gases were delivered from a compressed gas cylinder (Praxair) and continuously injected through the purge ports until all other sample cell constituents were displaced through the open inlet port. To corroborate the results, the cavity was also filled with Ar (99.998%), which has slightly larger scattering cross-sections than that of N_2.

Figure 3a shows cavity-enhanced transmission spectra with the optical cavity filled with N_2, He, and Ar, each averaged over a 15 min time period. The intensity difference due to scattering by Ar and N_2 was more pronounced in the case when the sample cell was filled with He (Figure 3a, inset), as expected based on their relative cross-sections (Thalman et al., 2014).

Figure 3b shows the reflectivity spectra calculated using Eq. (6). The reflectivity curves are essentially smooth continua, with maximum reflectivity of ~99.98%. The relative difference between the reflectivity calculated from the ratios of Ar/He and N_2/He was $< 1.6\times10^{-6}$ in the 480–530 nm range. Arbitrarily, the N_2/He mirror curve was chosen to calculate the mirror reflectivity for the remaining data analysis in this work with the exception of the scattering cross-sections of N_2 and CO_2 (see Sect. 4.1.1 and 4.1.5) for which the Ar/He pair was used. The observed reflectivity corresponds to a total path length ($\approx d/(1-R)$) of 5.5 and 6.3 km near 485 nm and 520 nm, respectively. Intermittent measurements of mirror reflectivity showed that it remained unchanged throughout this work; in particular, no difference in reflectivity was found prior to and following the ORCA campaign.

The overall uncertainty in the measured mirror reflectivity was ±2.3%, resulting from addition by quadrature of a ±1% uncertainty in the N_2 scattering cross-section (Peck and Khanna, 1966), a ±2% uncertainty in the He cross-section (Washenfelder et al., 2008; Min et al., 2016), ±0.4% uncertainty in temperature, ±0.1% uncertainty in pressure, and ±0.1% random noise due to photon counting statistics.

3.3 Determination of the effective optical absorption path

When sampling ambient air, ~~K~~knowledge of the path length over which sampled air is present (d_0) and the associated correction factor R_L is essential~~ in experiments involving resonant optical cavities, especially~~ for accurate IBBCEAS measurements when purge~~ing~~ gases are used to maintain clean mirrors as in this work. ~~If the mirror reflectivity R is~~

~~known, d_0 can be determined by measuring the extinction of a known amount of a strongly absorbing, non-reactive gas with known absorption cross-section, which is sampled through the inlet port. Combining Eq. (1) and Eq. (2) and rearranging gives an expression for d_0:~~

~~$d_0 = \frac{\delta I(\lambda)}{\sigma N}\left(1 - R(\lambda) + d\alpha_{Ray}(\lambda)\right)$ (7)~~

~~Here, $\delta I(\lambda) = [I_0(\lambda) - I(\lambda)]/I(\lambda)$. In this work, we used water vapour and the absorption cross-section of H_2O from (Coheur et al., 2002) to determine $R_L = d/d_0$. A saturated gas stream of water vapour was generated by bubbling air through a water reservoir at a temperature of 298 K and pressure of 0.88 atm. Using Eq. (4), d_0 was found to be 73.2±0.7 cm, in agreement with the physical dimension (~73 cm) of the CEAS sample path. With d = 102.0 cm, this gives R_L = 1.39±0.01.~~The effective cavity length, d_0, was determined by sampling pure oxygen and monitoring the O_2 dimer (Duan et al., 2018). This experiment was performed in the 350 - 390 nm wavelength region using highly reflective mirrors and an LED (Thorlabs M365LP1) suitable for this wavelength region, though in principle it could have been performed in the cyan region as well since both spectral regions contain O_4 absorption lines. Following Duan et al. (2018), d_0 is given by

$$d_0 = d \times \frac{[O_2]_{on}}{[O_2]_{off}} \quad (7)$$

where $[O_2]_{on}$ and $[O_2]_{off}$ are the $[O_2]$ retrieved using cross-sections by (Thalman and Volkamer, 2013) with or without the purge flows. Consistent results were obtained when a constant mixing ratio of NO_2 was sampled (and purge flows were turned on and off) and from the ratio of expected absorption by O_4 (calculated from the square of the number density of O_2 and the O_4 cross-section) relative to the observed O_4 absorption, though the latter may be less accurate as the absorption changes non-linearly in the region where purge and sample gases mix and requires accurate knowledge of mirror reflectivity.

At a sample flow rate of 2.0 slpm, a purge flow rate of 0.1 slpm, and cell pressure of 870 hPa, we determined $R_L = d/d_0$ = 1.28±0.05 (1σ precision stated) with an accuracy of ±5%. This R_L value is smaller than calculated from the ratio of the inter-mirror distance d to the distance between the inlet and outlet of the sample flow (~1.39), which suggests that sampled air partially mixes into the purge volume. At a volumetric flow rate of 11 liters per minute as deployed during ORCA, we observed R_L = 1.20±0.07 (1σ precision).

3.4 Reference absorption cross-sections

Figure 1 shows trace absorbers in the 480–530 nm window calculated as extinction ($\alpha_i(\lambda) = \sigma_i(\lambda)N$) for typical atmospheric mixing ratios. CEAS analysis was performed using the high-resolution NO_2 absorption cross-section of Voigt et al. (2002) and the cross-sections of Spietz et al. for OIO (Spietz et al., 2005) and I_2 (Spietz et al., 2006), respectively. The NO_2 cross-section was convolved with the instrument function corresponding to a sharp peak line (540.06 nm) in the emission spectrum of the Hg(Ne) calibration lamp (Figure S2), which was also used to calibrate the wavelength scale of the spectrometer.

The IBBCEAS ~~spectrometer~~ instrument's resolution was 0.33 nm in the 480–530 nm window, whereas the NO_2 literature spectrum was recorded at a higher resolution of better than 0.005 nm (Voigt et al., 2002). A ~~C~~convolved~~ing~~ ~~the~~ NO_2 reference spectrum ~~effectively degraded the high-resolution spectrum but~~ was ~~required~~ used for the least-squares analysis. The literature cross-sections of I_2 and OIO (Spietz et al., 2005; 2006) at a resolution of 0.59 nm were not convolved because their resolution was lower than that of the IBBCEAS instrument.

The NO_2 absorption cross-section is somewhat pressure-dependent, which is important considering that the IBBCEAS instrument was operated at ~~~350 Torr~~466 hPa in the field. Voigt et al. (2002) reported cross-sections at 1333~~1000~~ and ~~100~~ 133 ~~Torr~~ hPa (in N_2). Following convolution to the ~~(relatively) low resolution~~ IBBCEAS instrument, these differences were judged to be small (2 – 5% in the 480 – 530 nm range).

3.5 Spectral fitting

The DOAS intelligent system (DOASIS; (Kraus, 2003)) was used to retrieve gas-phase concentrations. Optical extinction data collected in laboratory experiments were fitted using the literature absorption spectra (Sect. 3.3) and a third-degree polynomial to represent broad-band processes (e.g., temperature fluctuation, Mie scattering and extinction by aerosols). The "spectral shifting" setting in DOASIS was set to ±0.2 nm, and stretching was disallowed. ~~The contributions of water vapor to the optical extinction was neglected since the relative humidity of the air sampled during the background measurement was the same as during the measurement of NO_2 or I_2.~~

The same parameters were used to fit the data from the ORCA field campaign except that in an effort to minimize the fit residuals, the convoluted absorption cross-section of H_2O based on the high-resolution data by (Coheur et al., 2002) was also included in the fit. The contributions of water vapor to the optical extinction was ~~neglected~~ small since the relative humidity of the air sampled during the background measurement was the same as during the measurement of NO_2 or I_2.Further, the optical extinction (α) values, as per Eq. (1), were smoothed using a fourth order polynomial filter (Savitzky and Golay, 1964). Smoothing improved the root mean square (RMS) of the residuals and the fit uncertainty by a factor of ~2 (Figure S3).

3.6 Description of CRDS instrument

The IBBCEAS instrument quantified NO_2 in parallel to a blue diode laser CRDS instrument, which has been described previously (Paul and Osthoff, 2010; Odame-Ankrah, 2015). Briefly, mixing ratios of NO_2 are quantified by optical absorption using a continuous wave (cw) laser whose emission is centered at 405 nm (Power Technology IQµ2A105, Little Rock, AR, USA). The radiation is square-wave (on/off) modulated at a repetition rate of 1 kHz (50% duty cycle) and enters a 111 cm long stable resonator formed by two highly reflective mirrors (2.54 cm diameter; Advanced Thin Films, Boulder, CO, USA) in a concentric configuration. The cavity output is coupled into a 200 µm diameter, 0.22 numerical aperture, multimode optical fibre (Thorlabs M25L01) illuminating a photomultiplier tube (Hamamatsu Photonics H9433-03MOD, Japan). The ring-down decay traces are co-added and fitted to an exponential using the discrete sums algorithm described by Everest and Atkinson (2008).

The CRDS NO_2 channel was operated in parallel to a CRDS NO_x channel, to which a small flow of O_3 in O_2 was added to convert NO to NO_2, similar to the method described by Fuchs et al. (2009). Following the O_3 addition point, the sampled air passed through a coiled reaction chamber with a total residence time of ~7 s to ensure complete titration and a linear response up to ~100 ppbv of NO (Odame-Ankrah, 2015). An identical chamber was added to the NO_2

channel to match the response times of the two channels. Mixing ratios of NO_2 and NO_x measured by CRDS were accurate within ±10% (Osthoff et al., 2017).

3.7 Generation and delivery of ~~calibration~~ gases

Figure 2b shows the setup for delivery and sampling of NO_2. NO_2 was generated by mixing the output of a standard NO cylinder (100.2±1.0 ppmv in N_2; Scott-Marrin, Riverside, CA, USA) delivered using a 20 sccm all metal MFC (MKS Instruments 1479A) with O_3 produced by illuminating a flow of O_2 (Praxair) with a 254 nm Hg pen-ray lamp (Jelight, Irvine, CA, USA) and dilution with zero air.

Iodine was purchased in a solid crystalline form (≥99.8%, Sigma-Aldrich, Oakville, ON, Canada). Small amounts were placed in a Teflon™ permeation tube (VICI Metronics, Poulsbo, WA, USA); these tubes were sealed on both ends with PTFE plugs compressed with stainless steel rings and were (individually) placed in a temperature-controlled permeation chamber (Vici Metronics, model 120-1) operated with a constant air flow of ~0.3 litres per minute. The flow from the permeation chamber was diluted with zero air, yielding iodine concentrations in the range of ~70 pptv up to 21 ppbv depending on chamber temperature and permeation tube dimensions (i.e., wall thickness and length).

Ar, CO_2, CH_4, N_2, O_2, air and He were delivered from compressed gas cylinders (Praxair) in the same manner as described in section 3.2.

3.8 ORCA field campaign

The IBBCEAS instrument was operated alongside the CRDS during a four week long field intensive conducted at the Amphitrite Point Observatory (APO) on the west coast of Vancouver Island, British Columbia, Canada (Tokarek et al., 2017). The APO was established as a marine background monitoring site but is sporadically impacted by NO_x emissions mainly from ship and boat traffic in the region (McKendry et al., 2014).

The IBBCEAS and CRDS instruments sampled, in parallel, from a 5.5 m long common 0.63 cm o.d. and 0.48 cm i.d. FEP Teflon™ inlet line, flooded with calibration gases and zero air ~~in~~ at regular intervals. Zero air was generated using a custom-built zero air generation system (Odame-Ankrah, 2015), which delivered air at ambient relative humidity that was free of trace gases such as NO_2, NO, I_2, or O_3. This approach minimized absorption by H_2O from the extinction spectra which can create artifacts (Bahrini et al., 2018). A flow restriction was placed upstream of the inlet filter. When the IBBCEAS instrument was operated at a flow rate of 5 slpm, an average (±1σ) sample cell pressure of ~~355~~ 473 (±~~17~~23) ~~Torr~~ hPa and inlet residence time of 2.3 s were achieved. The cell pressure varied over short time periods with a standard deviation of ±~~1.8~~2.4 ~~Torr~~hPa. A PAN-GC (Tokarek et al., 2014), commercial NO/NO_y and O_3 instruments (Thermo 42i and 49i), as well as a 662 nm diode laser N_2O_5 channel (Osthoff et al., 2017) also sampled off this common inlet line, resulting in all instruments periodically sampling a variety of calibration gases.

The IBBCEAS transmission spectrum was integrated for 9 s, resulting in ~90% saturation of the CCD at 500 nm. Dark spectra (to characterize the spectrometer offset) were acquired daily with the same integration time (9 s). Wavelength calibration spectra of the Hg(Ne) lamp were collected daily over a period of 2 min and showed that the spectrometer wavelength scale remained relatively unchanged (±0.02 nm) over the region of interest. The mirror reflectivity was measured prior to and after the campaign and agreed within ±(1×10^{-7}). Data were averaged over 60 s post-campaign prior to analysis.

4 Results

4.1 Measurements of cross-sections of pure gases

The extinction cross-sections of N_2, CO_2 (based on mirror reflectivity determined from the Ar/He ratio of scattering coefficients), O_2, air, Ar, and CH_4 (based on mirror reflectivity determined from the N_2/He ratio of scattering coefficients) in the 480–535 nm wavelength range are shown in Figure 4; values at selected wavelengths are summarized in Table 1. For N_2, Ar, and CO_2, the extinction is due to scattering only. In contrast, the spectra of O_2, air and CH_4 include optical losses due to absorption in addition to scattering. The systematic uncertainty of these data was ±2.5%; the systematic errors arise mainly from uncertainties in the mirror reflectivity (±2.3%, see Sect. 3.2) and errors in the scattering cross-section terms in Eq. (3). The precision of the data (calculated after subtracting a 4th order polynomial from the observed cross-sections) varies from ±2.5% for the CO_2 data shown in Figure 4e to ±0.9% for the N_2 data shown in Figure 4b.

4.1.1 Nitrogen

Figure 4b shows the measured scattering cross-sections of N_2 at a temperature of 299.0±0.1 K and pressure of ~~660.0~~879.7±0.7~~5~~ ~~Torr~~ hPa between 480 and 535 nm. Superimposed are *n*-based cross-sections predicted using Eq. (5), data by (Peck and Khanna, 1966), and the King correction factor by (Bates, 1984). In addition, the single wavelength CRDS measurement at 532.2 nm by (Sneep and Ubachs, 2005) and the nephelometer data of (Shardanand and Rao, 1977) are shown.

The IBBCEAS data are marginally larger than the *n*-based prediction, with the percent difference ranging from +0.2% at 525.07 nm to +1.3% at 485.03 nm (Table 1). These differences are well within the margin of measurement error (±2.5%), set in this case by the accuracy of the scattering cross-sections of He (±2%) and Ar (<1%). The IBBCEAS data differ from the CRDS data of (Sneep and Ubachs, 2005) at 532.2 nm by +7.1%, though the error bars overlap; the measurement uncertainty of the CRDS data alone is ±9.4%. The IBBCEAS measurements also differ by +4.6% at 488.0 nm and by +8.8% at 514.5 nm) from the data of (Shardanand and Rao, 1977) but are within combined measurement error (±2.5% and ±11%, respectively).

4.1.2 Argon

The scattering cross-sections of Ar at 299.0±0.1 K and 879.7±0.7 hPa~~660.0±0.5 Torr~~ are shown in Figure 4b. Superimposed are the *n*-based cross-sections calculated using data from (Peck and Fisher, 1964) and the King correction factor from (Bates, 1984). The single-wavelength measurement of (Sneep and Ubachs, 2005) and the nephelometer data of (Shardanand and Rao, 1977) are shown for comparison.

The observed scattering cross-sections are marginally larger than the *n*-based prediction, by +1.3% at shorter wavelengths and +0.21% at 515.06 nm (Table 1). These differences are within measurement error of the IBBCEAS instrument (±2.5%) inferred from the accuracy in the determination of the scattering cross-sections of He (±2%) and N_2 (±1%) used in the determination of the mirror reflectivity. The IBBCEAS cross-sections differ from the CRDS data by (Sneep and Ubachs, 2005) at 532.2 nm and are well within either measurement error bar (Figure 4b). In contrast, the CEAS values differ from the nephelometer data by -10.8% at 488.0 nm and by -5.1% at 514.5 nm, though they are within the ±11% uncertainty of the nephelometer.

4.1.3 Oxygen

The extinction cross-sections of O_2 (at a temperature of 299 K and a pressure of ~~660~~ 880 ~~Torr~~hPa) are shown in Figure 4c next to the *n*-based predictions based on (Bates, 1984) and the nephelometer measurements of (Shardanand and Rao, 1977). The IBBCEAS data show two absorption bands due to the oxygen dimer, O_4, centered at 477 nm and 532 nm (Thalman and Volkamer, 2013). In the 490 – 515 nm wavelength interval, the contribution of these absorption bands to the total extinction is negligible (<0.2% at 515 nm), i.e., the extinction is dominated by scattering. In this region, the observed cross-sections are slightly larger than the *n*-based data of (Bates, 1984): the differences range from +8.3% at 495.08 nm to +2.5% at 515.06 nm (Table 1). Relative to the nephelometer measurements, the IBBCEAS data differ by +8.7% at 488 nm and by +15.3% at 514.5 nm.

We calculated the absorption cross-section of O_4 by subtracting the scattering cross-section of (Bates, 1984), upshifted by $+3.86\times10^{-28}$ cm^2 $molecule^{-1}$ (i.e., by 6%) to match the *n*-based data to the observed extinction from 487 nm to 516 nm, from the extinction shown in Figure 4c, and dividing by the number density of O_2 (2.13×10^{19} molecules cm^{-3}). The result is shown in Figure S4. The error for this absorption cross-section calculation is estimated at ±8.5%, with the largest source of error being the correction to the scattering cross-section extrapolated from the region where absorption is negligible, For the smaller band between 520 and 540 nm, the observed cross-section of $(1.08\pm0.09)\times10^{-46}$ cm^5 $molecule^{-2}$ is in agreement with recent room-temperature measurements by other groups (Table S1). For the larger band between 467 and 485 nm, the peak cross-section of $(6.2\pm0.5)\times10^{-46}$ cm^5 $molecule^{-2}$ is smaller than that reported in recent measurements (Thalman and Volkamer, 2013; Sneep et al., 2006), though the shape of the peak is identical and the error bars overlap.

4.1.4 Air

Figure 4d shows the extinction spectrum of ultrapure air ("zero" grade, Praxair) at a temperature of (298.5±0.1) K and pressure of 879.7±0.7 hPa ~~(660.5±0.5) Torr~~. Superimposed is the *n*-based prediction from the refractive index data of (Penndorf, 1957) and King correction factor from (Bodhaine et al., 1999).

The sample cylinder contains a sufficiently high quantity of O_2 (~19.5% by volume, Praxair) for O_4 absorption bands to appear at 477.5 and 531.5 nm. In the 495 - 515 nm wavelength region, the cross-sections observed by IBBCEAS are slightly larger than the *n*-based prediction, by +4.0%, +3.0%, and +6.8% at 495, 505, and 515 nm, respectively (Table 1).

4.1.5 Carbon dioxide

Figure 4e shows the scattering cross-sections of CO_2 at (299.0±0.1) K and (879.7±0.7 hPa~~660.0±0.5) Torr~~ for the 475 – 540 nm wavelength interval. ~~–~~Superimposed are the *n*-based prediction based on (Bideau-Mehu et al., 1973), nephelometer measurements (Shardanand and Rao, 1977), and a CRDS measurement at 532.2 nm (Sneep and Ubachs, 2005). The observed scattering cross-sections differ from the *n*-based prediction by -2.9%, +2.4% and -2.8% at 485 nm, 505 nm, and 525 nm, respectively (Table 1). In contrast, the CRDS measurement at 532.2 nm, which has a relatively high uncertainty of ±6.5% at the 1σ level, is 11% lower than the IBBCEAS measurement. The nephelometer measurements (Shardanand and Rao, 1977), on the other hand, are significantly larger than the other data shown and appear to be in error.

4.1.6 Methane

Figure 4f shows the extinction spectrum of CH_4 (research grade, 99.97%) for the 475 – 550 nm interval at (298.5±0.1) ~~–~~K and 879.7±0.7 hPa ~~(660.5±0.5) Torr~~. The CH_4 spectrum in this region contains a number of combination and overtone absorption bands near 484.7, 486.1, 509.6, 522.0, and 543.4 nm that have been assigned by (Giver, 1978). These bands are relevant to studies simulating the atmospheres of Jovian planets (e.g., Uranus, Neptune) and Saturn's moon Titan that contain CH_4 (Karkoschka, 1994). Superimposed are CRDS data by (Sneep and Ubachs, 2005) and the *n*-based scattering cross-sections, calculated using the parameterization by Sneep and Ubachs, and refractive index data from (Hohm, 1993), assuming a depolarization ratio of unity and nephelometer data by (Shardanand and Rao, 1977) extrapolated using Eq. (5) (dashed line). In spite of the many absorption bands, there are small windows where the optical extinction appears to be dominated by scattering and a comparison with literature is feasible. There is very little difference (within combined measurement errors) between IBBCEAS and interpolated nephelometer data at those wavelengths. At 492.06 nm and 527.28 nm, for example, the data are within -0.07% and 0.17%, respectively (Table 1). There is also reasonable agreement between the IBBCEAS and CRDS data 532.2 nm, which differ by 4.7% but compares well with the total IBBCEAS uncertainty of 4.6% for CH_4.

4.2 Measurement of trace gas mixing ratios

4.2.1 Nitrogen dioxide

An example of a spectral retrieval for NO_2 in ambient air ~~CEAS measurement~~ is shown on Figure 5a. The figure shows the measured optical extinction (α) for a routine calibration period during the ORCA campaign on 22 Jul~~,~~ 2015 at 11:52:07 to 11:57:02 (UTC). Superimposed is a fit determined with DOASIS. An NO_2 mixing ratio of (11.6 ± 0.4) ppbv was retrieved, corresponding to an ambient air mixing ratio of (13.9±1.0) ppbv when R_L is factored in. The residual spectrum is lacking structure, indicating that other absorbers are not significant in this wavelength region.

During the ORCA campaign, the inlet of the IBBCEAS instrument (and of the CRDS instrument, which sampled in parallel) was overflowed every 30 min with a standard gas mixture of ~20 ppbv NO_x containing up to 16 ppbv of NO_2 in zero air and with ~130 ppbv of NO added to ambient air. The zerfo air was generated using a scrubber constructed in-house that delivered air with a similar moisture content as ambient air. A subset of these data (and the ambient air data sampled in between) is shown in Figure 6a.

High concentrations of NO in air are prone to oxidation (by O_3 and, to a lesser degree, by O_2) to NO_2 (Atkinson et al., 2004). Because the CRDS had a longer inlet residence time (7 s) than the IBBCEAS instrument (2.3 s), it observed greater conversion of NO to NO_2 when the high NO concentration standard was sampled in an ambient air matrix. On the other hand, when the lower concentration NO_x standard was sampled in O_3-free air, the two instruments ~~agreed well~~were in better agreement (Figure 6a).

Shown in Figure 7a is a scatter plot of all of the NO_x calibration data. This plot shows a linear relationship with a slope of 1.11±0.01~~0.923±0.009~~, an intercept of 0.2±0.1~~0.18±0.09~~ ppbv, and r^2 = 0.975. The slope of the line in Figure 7a reveals ~~7.7%~~an 11% systematic difference in the measurement of the calibration standard.

~~In ambient air, t~~The median NO_2 mixing ratio during ORCA was 1.24 ppbv. Shown in Figure 6b is a time series of a subset of ambient air NO_2 measurements. The IBBCEAS NO_2 data clearly exhibit more scatter than the CRDS NO_2 data and occasionally fall below zero. For ambient air data collected on 18-19 Jul 2015, ~~T~~the scatter plot of IBBCEAS and CRDS NO_2 data (Figure 7b) has the same slope (1.12±0.02) as that shown in Figure 7a, while the scatter plot of the entire campaign has a slope of 1.02±0.01 (Figure 7C)~~(Figures 7b and 7c) suggest that the CRDS data were systematically higher than the CEAS data, by 15% when sampling ambient air (Figure 7c)~~. When data are filtered by removing all IBBCEAS points below a factor of three times the standard deviation of a blank measurement for 60 s (~1 ppbv; see Sect. 4.3), the slope of the scatter plot, when forced through an intercept of zero, is ~~0.98±0.01~~1.18±0.01 (r^2 = ~~0.070~~0.70), suggesting that the IBBCEAS are biased high.

4.2.2 ~~Molecular i~~Iodine species (I_2, OIO)

Figure 5b shows an example ~~of an~~retrieval for I_2~~ measurement~~. The extinction spectrum was recorded during the ORCA campaign on 18 Jul 2015, when I_2 from a permeation source had been added to the inlet and represents a 60 s average. A mixing ratio of (10.1±0.2) ppbv was retrieved in this example.

Figure S5 shows spectra of laboratory generated I_2 samples and their respective absorption spectra, fits, and residuals. ~~The smallest amount of I_2 that was produce without dilution of the permeation chamber output flow was ~21 pptv.~~ Fit results near 20 pptv showed large residuals (±27%) indicating that the IBBCEAS instrument was near its detection limit.

A sample time series of laboratory I_2 measurements (30 s averaged data) is shown in Figure S6. Gas streams containing I_2 were generated using four permeation tubes of different wall thickness, that were exchanged while the output of the permeation was bypassed and the IBBCEAS sampled zero air. The IBBCEAS instrument responded rapidly to concentration changes: for example, at 22:05, the response 30 s after "zeroing" was 10% of the preceding value, indicating that memory effects (from slow adsorption / desorption kinetics of iodine on the inner walls of the inlet) were negligible.

Figure S7 shows a sample time series of I_2 mixing ratios during the ORCA campaign. Concentrations of I_2 (and of OIO, not shown) in ambient air were below the instrument's detection limits. At 22:30 UTC, I_2 from a diffusion source was added to the inlet. While the transmission of iodine through inlets was not systematically investigated in this work, ~~T~~the square-wave response and quick rise and fall times suggest the absence of inlet transmission losses.

4.3 Accuracy and limits of detection

The accuracy of the IBBCEAS NO_2 measurement is influenced by uncertainties in the absorption cross-section of NO_2 (±3%) (Voigt et al., 2002), fit errors ±(3 – 5%~~)~~, which can be reduced to ±(2 – 4)% by smoothing), scattering cross-sections, i.e., mirror reflectivity (±2.5%~~) (see;~~ Sect. 3.2 and 4.1), R_L (±5%; Sect. 3.3), and ~~calibration~~ errors in the mass flow controller reading (±1%), sample cell pressure readout (±0.5%), and temperature measurement (±0.7%). The total uncertainty, expressed as the square root of the individual errors summed in quadrature, is ±(~~5.5~~7 – ~~7.6~~8)%. Not included in this estimate are errors arising from interpolation of infrequent mirror reflectivity and R_L determinations in the field.

The limits of detection (LOD) were assessed through Allan deviation analyses (Werle et al., 1993). For NO_2 sampled at a flow of 1.5 slpm and cell pressure of ~~668 Torr~~890 hPa, the Allan deviation was ±~~278~~ 360 pptv for 10 s data, ±~~105~~ 135 pptv for 60 s data, and ±~~49~~ 63 pptv for 5 min data averages (Figure 8a). At the higher sample flow of 5 slpm and reduced cell pressure of ~~350 Torr~~466 hPa used during the ORCA campaign, the ~~Allen~~ Allan deviation was ±164~~137~~ pptv for 334 s data (Figure S8).

For I_2 in laboratory-generated samples~~ under optimal conditions~~, typical 1σ fit errors ~~(when integrated over~~ for 60 s averaged~~)~~ data were ±~~5.8~~7 pptv ~~for~~ when ~~21~~ 21 pptv I_2 were sampled and ±~~7~~ 9 pptv ~~for~~ when ~~350~~ 544 pptv I_2 were sampled (Figure S6). The accuracy ~~for~~ of I_2 data is, in principle, of similar magnitude to that of the NO_2 data, except that it also depends on knowledge of inlet transmission efficiency, which was not assessed in this work~~was (5.4 – 6.4)%, with main contribution from error in the high-resolution absorption cross-section of I_2 (Spietz et al., 2006)~~. The Allan deviation plot in Figure 8b demonstrates 1σ measurement precisions for I_2 of ±~~38~~ 49 pptv for 60 s and ±~~16~~ 22 pptv for 5 min averaged data. During ORCA, the 1σ precisions were ±~~100~~ 120 pptv for 60 s and ±~~50~~ 60 pptv for 5 min data, respectively.

For OIO, the Allan deviation analysis gives 1σ measurement precisions of ±5.7~~4.6~~ pptv for 60 s and ±2.3~~1.8~~ pptv for 5 min averaged data (Figure S9b) in the laboratory.

5 Discussion

The IBBCEAS instrument described in this work adds to a growing number of instruments designed for measurement of atmospheric trace gases (Table 2). It differentiates itself foremost through its ~~unique~~ wavelength region, where several trace gases of atmospheric interest (e.g., NO_2, I_2, IO, and OIO) absorb (Figure 1). Measurements of optical absorption in the cyan region enable simultaneous quantification of I_2, and, potentially, IO, and OIO in a single channel. Currently, such measurements require multiple detection channels, for example quantification of I_2 and OIO mixing ratios using the 525 – 555 nm range and those of IO the 420 – 460 nm window in a separate channel (Vaughan et al., 2008). A reduction of channels and LEDs corresponds to savings in space and power requirements, important considerations in the field.

As such, this paper has laid some of the ground work for future measurements in the cyan spectral region, in that we measured relevant scattering and absorption cross-sections of pure gases (see S.I.). Such information is needed to determine mirror reflectivity and is useful to probe the consistency of scattering cross-sections reported for this wavelength region (of which there have been relatively few) and, hopefully, improve upon their accuracy, to better describe transmission of radiation through the atmosphere.

Scattering cross-section measurements for non-absorbing gases agree with ~~all~~ recent literature values (Figure 4 and Table 1). For example, the IBBCEAS scattering cross-section measurements agree, within the combined experimental uncertainties (1σ), with the CRDS data by (Sneep and Ubachs, 2005) at 532.2 nm for N_2, Ar, CO_2, and CH_4, and with the nephelometer measurements of (Shardanand and Rao, 1977) at 488.0 and 514.5 nm for N_2, Ar, O_2, and CH_4. For CO_2, the IBBCEAS data closely match the data by ~~Bideau-Mehu et al.~~ (Bideau-Mehu et al., 1973) and recent data by (He et al., 2018); the older data by (Shardanand and Rao, 1977), in contrast, appear high (Figure 4e).

In the case of CH_4, to lesser extent, O_2 and, air, the analysis is complicated by absorption lines. For O_2, our data and derived collisional-induced absorption cross-sections agree with literature (Table S1). For regions that appear to be free of absorption bands, the IBBCEAS data for CH_4 (Figure 4f) agree with cross-section measurements of (Shardanand and Rao, 1977) but not with the more recent work of (Hohm, 1993) whose data appear high. The CRDS data point by (Sneep and Ubachs, 2005) is on a shoulder of a large absorption band and hence not a valid measurement of scattering but extinction cross-section; their data agrees with the extinction cross-section observed in this work. Accurate knowledge of the scattering cross-section of CH_4 is important to the study of planetary bodies with atmospheric content of CH_4 such as Saturn's moon Titan. Future studies should re-examine the scattering cross-section measurements of CH_4 to resolve the reported differences.

The detection limit for NO_2 achieved under laboratory conditions in this work (~~49~~ 63 pptv for 5 min data) is ~~compared~~ of similar magnitude ~~to~~ as those by instruments operated in other wavelength regions (Table 2). However, the IBBCEAS measurement precision in this work was surpassed by the more mature blue diode CRDS, though future upgrades (~~e.g., more highly reflective mirrors, more sensitive spectrometer, etc.~~see below) may improve the IBBCEAS precision. On the other hand, the IBBCEAS may ultimately be more accurate. Unlike IBBCEAS where all absorbing molecules are incorporated in the fit, the measurement of NO_2 by blue diode laser CRDS is prone to potential interference from molecules that absorb at 405 nm such as glyoxal and methyl glyoxal (Fuchs et al., 2009). For example, Fuchs et al. estimated that the presence of glyoxal could introduce an interference of ~1% in polluted and up to 10% in forested environments (Fuchs et al., 2009). The low precision of the data in the scatter plot shown in Figure 7c prevents us from drawing a definitive conclusion as to the magnitude of such interferences. Still, future comparisons of IBBCEAS and blue diode CRDS measurements of ambient NO_2 should be conducted. The data presented in this manuscript show that accurate measurements of NO_2 in ambient air by a cyan IBBCEAS are possible. An important parameter in any IBBCEAS measurement is the effective cavity length. Duan et al. recently summarized past practices in its determination and found that these practices vary considerably between groups (Duan et al., 2018). In this work, the necessary correction (R_L = 1.28 at 2.0 slpm sample flow rate) differed substantially from the physical dimension of the cell (1.39), underlining its importance for accurate measurements. However, it is unclear to what extent R_L varies between molecules which will need to be investigated. To improve the accuracy of future measurements, we will deploy more frequent zeroing and verify R_L periodically, for example by periodic sampling of molecular oxygen and measuring O_4 concentration.

The sensitivity for I_2 and OIO (~~16~~ 22 and ~~1.8~~2.3 pptv for 5 min averaged data under laboratory conditions) suffices for their quantification in environmental chamber studies (Dixneuf et al., 2009). Further, these LODs are below maximum I_2 and OIO abundances reported at Mace Head, Ireland, of 94 and 13 pptv (Bitter et al., 2005) and 61 and 9.2 pptv (Peters et al., 2005), respectively, but above the maximum I_2 level of 4 pptv reported in California (Finley and Saltzman, 2008). This implies that iodine species on the West coast of British Columbia, Canada, might have been detected if the instrument had been operated optimally. Even then, the LOD for I_2 of ~~76~~ ~100 pptv (2σ, 60 s average) is larger than the LOD of 26 pptv (2σ, 60 s average) reported by Vaughan et al. (2008). This suggests that improvements are possible. ~~Below we discuss potential instrument modifications to improve the detection limit and sampling of iodine species in future field deployments.~~

One area for improvement is the thermal management of the LED. Its intensity and wavelength drifts with temperature, necessitating temperature stabilization to achieve a constant emission profile. In this work, the cyan LED was stabilized by mounting a single Peltier thermoelectric module and thermocouple between the heat sink and the LED. When evaluated in the climate-controlled laboratory, this yielded a cavity emission profile that varied along the entire wavelength range (446.9–563.2 nm) of the spectrometer by ±15 counts (Figure S10). At 500 nm, this corresponded to an absorption coefficient of $\pm 1\times10^{-9}$ cm^{-1}. During the field deployment, however, the LED was subject to greater output fluctuations, since the trailer temperature was not as well controlled as in the laboratory, and thermal gradients between the LED and thermocouple may have come into play.

When deployed in the field, the performance of the IBBCEAS instrument was also compromised by variable cell pressure which added noise to the optical extinction, caused in part by the large pressure drop from ~~~760~~ 1013 to ~~~350 Torr~~467 hPa. Furthermore, we discovered post-campaign that the alignment of the round-to-linear fiber bundle is very sensitive to vibrations, which would have added additional noise during the field campaign. In future deployments, improved pressure, temperature and vibrational stabilization of the sample cell (as it is common in aircraft deployments, for example) and instrument will be paramount.

Acknowledgments

This work was made possible by the financial support of the Natural Science and Engineering Research Council of Canada (NSERC) in the form of a Discovery grant, of the Canadian Foundation for Innovation (CFI) in the form of a LOF grant, and by the Government of Alberta's Advanced Education and Technology (AET) Small Equipment Grants Program (SEGP). The authors thank the Birrs and Thurbide groups at the University of Calgary for loans of CH_4 and CO_2 compressed gas cylinders used in this work.

References

Atkinson, R., Baulch, D. L., Cox, R. A., Crowley, J. N., Hampson, R. F., Hynes, R. G., Jenkin, M. E., Rossi, M. J., and Troe, J.: Evaluated kinetic and photochemical data for atmospheric chemistry: Volume I - gas phase reactions of O_x, HO_x, NO_x and SO_x species, Atmos. Chem. Phys., 4, 1461-1738, 10.5194/acp-4-1461-2004, 2004.

Axson, J. L., Washenfelder, R. A., Kahan, T. F., Young, C. J., Vaida, V., and Brown, S. S.: Absolute ozone absorption cross section in the Huggins Chappuis minimum (350 - 470 nm) at 296 K, Atmos. Chem. Phys., 11, 11581-11590, 10.5194/acp-11-11581-2011, 2011.

Bahrini, C., Grégoire, A.-C., Obada, D., Mun, C., and Fittschen, C.: Incoherent broad-band cavity enhanced absorption spectroscopy for sensitive and rapid molecular iodine detection in the presence of aerosols and water vapour, Optics & Laser Technology, 108, 466-479, 10.1016/j.optlastec.2018.06.050, 2018.

Ball, S. M., Hollingsworth, A. M., Humbles, J., Leblanc, C., Potin, P., and McFiggans, G.: Spectroscopic studies of molecular iodine emitted into the gas phase by seaweed, Atmos. Chem. Phys., 10, 6237-6254, 10.5194/acp-10-6237-2010, 2010.

Bates, D. R.: Rayleigh scattering by air, Planetary and Space Science, 32, 785-790, 10.1016/0032-0633(84)90102-8, 1984.

Bideau-Mehu, A., Guern, Y., Abjean, R., and Johannin-Gilles, A.: Interferometric determination of the refractive index of carbon dioxide in the ultraviolet region, Optics Communications, 9, 432-434, 10.1016/0030-4018(73)90289-7, 1973.

Bitter, M., Ball, S. M., Povey, I. M., and Jones, R. L.: A broadband cavity ringdown spectrometer for in-situ measurements of atmospheric trace gases, Atmos. Chem. Phys., 5, 2547-2560, 10.5194/acp-5-2547-2005, 2005.

Bluvshtein, N., Flores, J. M., Riziq, A. A., and Rudich, Y.: An Approach for Faster Retrieval of Aerosols,Äô Complex Refractive Index Using Cavity Ring-Down Spectroscopy, Aerosol Sci. Technol., 46, 1140-1150, 10.1080/02786826.2012.700141, 2012.

Bodhaine, B. A., Wood, N. B., Dutton, E. G., and Slusser, J. R.: On Rayleigh optical depth calculations, Journal of Atmospheric and Oceanic Technology, 16, 1854-1861, 10.1175/1520-0426(1999)016<1854:ORODC>2.0.CO;2, 1999.

Burkholder, J. B., and Talukdar, R. K.: Temperature-Dependence of the Ozone Absorption-Spectrum over the Wavelength Range 410 to 760 nm, Geophys. Res. Lett., 21, 581-584, 10.1029/93GL02311, 1994.

Chen, J., and Venables, D. S.: A broadband optical cavity spectrometer for measuring weak near-ultraviolet absorption spectra of gases, Atmos. Meas. Tech., 4, 425-436, 10.5194/amt-4-425-2011, 2011.

Coburn, S., Ortega, I., Thalman, R., Blomquist, B., Fairall, C. W., and Volkamer, R.: Measurements of diurnal variations and eddy covariance (EC) fluxes of glyoxal in the tropical marine boundary layer: description of the Fast LED-CE-DOAS instrument, Atmos. Meas. Tech., 7, 3579-3595, 10.5194/amt-7-3579-2014, 2014.

Coheur, P. F., Fally, S., Carleer, M., Clerbaux, C., Colin, R., Jenouvrier, A., Merienne, M. F., Hermans, C., and Vandaele, A. C.: New water vapor line parameters in the 26000-13000 cm^{-1} region, J. Quant. Spectrosc. Radiat. Transf., 74, 493-510, 10.1016/S0022-4073(01)00269-2, 2002.

Cuthbertson, C., and Cuthbertson, M.: The refraction and dispersion of neon and helium, P R Soc Lond a-Conta, 135, 40-47, 10.1098/rspa.1932.0019, 1932.

Dixneuf, S., Ruth, A. A., Vaughan, S., Varma, R. M., and Orphal, J.: The time dependence of molecular iodine emission from Laminaria digitata, Atmos. Chem. Phys., 9, 823-829, 10.5194/acp-9-823-2009, 2009.

Duan, J., Qin, M., Ouyang, B., Fang, W., Li, X., Lu, K., Tang, K., Liang, S., Meng, F., Hu, Z., Xie, P., Liu, W., and Häsler, R.: Development of an incoherent broadband cavity-enhanced absorption spectrometer for in situ measurements of HONO and NO_2, Atmos. Meas. Tech., 11, 4531-4543, 10.5194/amt-11-4531-2018, 2018.

Everest, M. A., and Atkinson, D. B.: Discrete sums for the rapid determination of exponential decay constants, Rev. Sci. Instrum., 79, 023108-023109, 10.1063/1.2839918, 2008.

Fiedler, S. E., Hese, A., and Ruth, A. A.: Incoherent broad-band cavity-enhanced absorption spectroscopy, Chem. Phys. Lett., 371, 284-294, 10.1016/s0009-2614(03)00263-x, 2003.

Finley, B. D., and Saltzman, E. S.: Observations of Cl_2, Br_2, and I_2 in coastal marine air, J. Geophys. Res., 113, D21301, 10.1029/2008jd010269, 2008.

Fuchs, H., Dubé, W. P., Lerner, B. M., Wagner, N. L., Williams, E. J., and Brown, S. S.: A Sensitive and Versatile Detector for Atmospheric NO_2 and NO_x Based on Blue Diode Laser Cavity Ring-Down Spectroscopy, Environm. Sci. Technol., 43, 7831-7836, 10.1021/es902067h, 2009.

Gagliardi, G., and Loock, H.-P.: Cavity-Enhanced Spectroscopy and Sensing, 1 ed., Springer Series in Optical Sciences, 179, Springer, Berlin, Heidelberg, 10.1007/978-3-642-40003-2, 2014.

Gherman, T., Venables, D. S., Vaughan, S., Orphal, J., and Ruth, A. A.: Incoherent broadband cavity-enhanced absorption spectroscopy in the near-ultraviolet: Application to HONO and NO_2, Environm. Sci. Technol., 42, 890-895, 10.1021/es0716913, 2008.

Giver, L. P.: Intensity measurements of the CH_4 bands in the region 4350 Å to 10,600 Å, J. Quant. Spectrosc. Radiat. Transfer, 19, 311-322, 10.1016/0022-4073(78)90064-X, 1978.

He, Q., Bluvshtein, N., Segev, L., Meidan, D., Flores, J. M., Brown, S. S., Brune, W., and Rudich, Y.: Evolution of the Complex Refractive Index of Secondary Organic Aerosols during Atmospheric Aging, Environm. Sci. Technol., 52, 3456-3465, 10.1021/acs.est.7b05742, 2018.

Hoch, D. J., Buxmann, J., Sihler, H., Pöhler, D., Zetzsch, C., and Platt, U.: An instrument for measurements of BrO with LED-based Cavity-Enhanced Differential Optical Absorption Spectroscopy, Atmos. Meas. Tech., 7, 199-214, 10.5194/amt-7-199-2014, 2014.

Hohm, U.: Experimental determination of the dispersion in the main linear dipole polarizability $\alpha(\omega)$ of small hydrocarbons and evaluation of Cauchy moments between 325 nm and 633 nm, Molecular Physics, 78, 929-941, 10.1080/00268979300100621, 1993.

Kahan, T. F., Washenfelder, R. A., Vaida, V., and Brown, S. S.: Cavity-Enhanced Measurements of Hydrogen Peroxide Absorption Cross Sections from 353 to 410 nm, J. Phys. Chem. A, 116, 5941-5947, 10.1021/jp2104616, 2012.

Karkoschka, E.: Spectrophotometry of the Jovian Planets and Titan at 300- to 1000-nm Wavelength: The Methane Spectrum, Icarus, 111, 174-192, 10.1006/icar.1994.1139, 1994.

King, L. V.: On the complex anisotropic molecule in relation to the dispersion and scattering of light, P R Soc Lond a-Conta, 104, 333-357, 10.1098/rspa.1923.0113, 1923.

Knight, G., Ravishankara, A. R., and Burkholder, J. B.: Laboratory studies of OBrO, J. Phys. Chem. A, 104, 11121-11125, 10.1021/jp002226u, 2000.

Langridge, J. M., Ball, S. M., and Jones, R. L.: A compact broadband cavity enhanced absorption spectrometer for detection of atmospheric NO_2 using light emitting diodes, Analyst, 131, 916-922, 10.1039/B605636A, 2006.

Langridge, J. M., Ball, S. M., Shillings, A. J. L., and Jones, R. L.: A broadband absorption spectrometer using light emitting diodes for ultrasensitive, in situ trace gas detection, Rev. Sci. Instrum., 79, 123110, 10.1063/1.3046282, 2008.

McKendry, I. G., Christensen, E., Schiller, C., Vingarzan, R., Macdonald, A. M., and Li, Y.: Low Ozone Episodes at Amphitrite Point Marine Boundary Layer Observatory, British Columbia, Canada, Atmosphere-Ocean, 52, 271-280, 10.1080/07055900.2014.910164, 2014.

Meinen, J., Thieser, J., Platt, U., and Leisner, T.: Technical Note: Using a high finesse optical resonator to provide a long light path for differential optical absorption spectroscopy: CE-DOAS, Atmos. Chem. Phys., 10, 3901-3914, 10.5194/acp-10-3901-2010, 2010.

Min, K. E., Washenfelder, R. A., Dubé, W. P., Langford, A. O., Edwards, P. M., Zarzana, K. J., Stutz, J., Lu, K., Rohrer, F., Zhang, Y., and Brown, S. S.: A broadband cavity enhanced absorption spectrometer for aircraft measurements of glyoxal, methylglyoxal, nitrous acid, nitrogen dioxide, and water vapor, Atmos. Meas. Tech., 9, 423-440, 10.5194/amt-9-423-2016, 2016.

Naus, H., and Ubachs, W.: Experimental verification of Rayleigh scattering cross sections, Opt. Lett., 25, 347-349, 10.1364/ol.25.000347, 2000.

Nitschke, U., Ruth, A. A., Dixneuf, S., and Stengel, D. B.: Molecular iodine emission rates and photosynthetic performance of different thallus parts of Laminaria digitata (Phaeophyceae) during emersion, Planta, 233, 737-748, 10.1007/s00425-010-1334-3, 2011.

Nitschke, U., Dixneuf, S., Schmid, M., Ruth, A. A., and Stengel, D. B.: Contribution of living and degrading kelp to coastal iodine fluxes, Mar. Biol., 162, 1727-1738, 10.1007/s00227-015-2699-4, 2015.

Odame-Ankrah, C. A.: Improved detection instrument for nitrogen oxide species, Ph.D., Chemistry, University of Calgary, http://hdl.handle.net/11023/2006, 10.5072/PRISM/26475, Calgary, 2015.

Osthoff, H. D., Odame-Ankrah, C. A., Taha, Y. M., Tokarek, T. W., Schiller, C. L., Haga, D., Jones, K., and Vingarzan, R.: Low levels of nitryl chloride at ground level: Nocturnal nitrogen oxides in the Lower Fraser Valley of British Columbia, Atmos. Chem. Phys., 18, 6293-6315, 10.5194/acp-18-6293-2018, 2017.

Paul, D., and Osthoff, H. D.: Absolute Measurements of Total Peroxy Nitrate Mixing Ratios by Thermal Dissociation Blue Diode Laser Cavity Ring-Down Spectroscopy, Anal. Chem., 82, 6695-6703, 10.1021/ac101441z, 2010.

Peck, E. R., and Fisher, D. J.: Dispersion of argon, Journal of the Optical Society of America, 54, 1362-1364, 10.1364/josa.54.001362, 1964.

Peck, E. R., and Khanna, B. N.: Dispersion of nitrogen, Journal of the Optical Society of America, 56, 1059-1063, 10.1364/josa.56.001059, 1966.

Penndorf, R.: Tables fo the refractive index for standard air and the Rayleigh scattering coefficient for the spectral region between 0.2 and 20.0 mu and their application to atmospheric optics, Journal of the Optical Society of America, 47, 176-182, 10.1364/josa.47.000176, 1957.

Peters, C., Pechtl, S., Stutz, J., Hebestreit, K., Honninger, G., Heumann, K. G., Schwarz, A., Winterlik, J., and Platt, U.: Reactive and organic halogen species in three different European coastal environments, Atmos. Chem. Phys., 5, 3357-3375, 10.5194/acp-5-3357-2005, 2005.

Saiz-Lopez, A., Plane, J. M. C., Baker, A. R., Carpenter, L. J., von Glasow, R., Gómez Martín, J. C., McFiggans, G., and Saunders, R. W.: Atmospheric Chemistry of Iodine, Chem. Rev., 112, 1773-1804, 10.1021/cr200029u, 2012.

Savitzky, A., and Golay, M. J. E.: Smoothing and Differentiation of Data by Simplified Least Squares Procedures, Anal. Chem., 36, 1627-1639, 10.1021/ac60214a047, 1964.

Schuster, G., Labazan, I., and Crowley, J. N.: A cavity ring down/cavity enhanced absorption device for measurement of ambient NO_3 and N_2O_5, Atmos. Meas. Tech., 2, 1-13, 10.5194/amt-2-1-2009, 2009.

Shardanand, and Rao, A. D. P.: Absolute Rayleigh scattering cross sections of gases and freons of stratospheric interest in the visible and ultraviolet regions, NASA TN D-8442, 1977.

Sneep, M., and Ubachs, W.: Direct measurement of the Rayleigh scattering cross section in various gases, J. Quant. Spectrosc. Radiat. Transfer, 92, 293-310, 10.1016/j.jqsrt.2004.07.025, 2005.

Sneep, M., Ityaksov, D., Aben, I., Linnartz, H., and Ubachs, W.: Temperature-dependent cross sections of O_2-O_2 collision-induced absorption resonances at 477 and 577 nm, J. Quant. Spectrosc. Radiat. Transf., 98, 405-424, 10.1016/j.jqsrt.2005.06.004, 2006.

Spietz, P., Gómez Martín, J. C., and Burrows, J. P.: Spectroscopic studies of the I_2/O_3 photochemistry: Part 2. Improved spectra of iodine oxides and analysis of the IO absorption spectrum, J. Photochem. Photobiol. A, 176, 50-67, 10.1016/j.jphotochem.2005.08.023, 2005.

Spietz, P., Gómez Martín, J., and Burrows, J. P.: Effects of column density on I_2 spectroscopy and a determination of I_2 absorption cross section at 500 nm, Atmos. Chem. Phys., 6, 2177-2191, 10.5194/acp-6-2177-2006, 2006.

Thalman, R., and Volkamer, R.: Temperature dependent absorption cross-sections of O_2-O_2 collision pairs between 340 and 630 nm and at atmospherically relevant pressure, Phys. Chem. Chem. Phys., 15, 15371-15381, 10.1039/c3cp50968k, 2013.

Thalman, R., Zarzana, K. J., Tolbert, M. A., and Volkamer, R.: Rayleigh scattering cross-section measurements of nitrogen, argon, oxygen and air, J. Quant. Spectrosc. Radiat. Transfer, 147, 171-177, 10.1016/j.jqsrt.2014.05.030, 2014.

Thalman, R., Baeza-Romero, M. T., Ball, S. M., Borrás, E., Daniels, M. J. S., Goodall, I. C. A., Henry, S. B., Karl, T., Keutsch, F. N., Kim, S., Mak, J., Monks, P. S., Muñoz, A., Orlando, J., Peppe, S., Rickard, A. R., Ródenas, M., Sánchez, P., Seco, R., Su, L., Tyndall, G., Vázquez, M., Vera, T., Waxman, E., and Volkamer, R.: Instrument intercomparison of glyoxal, methyl glyoxal and NO_2 under simulated atmospheric conditions, Atmos. Meas. Tech., 8, 1835-1862, 10.5194/amt-8-1835-2015, 2015.

Thalman, R. M., and Volkamer, R. M.: Inherent calibration of a blue LED-CE-DOAS instrument to measure iodine oxide, glyoxal, methyl glyoxal, nitrogen dioxide, water vapour and aerosol extinction in open cavity mode, Atmos. Meas. Tech., 3, 1797-1814, 10.5194/amt-3-1797-2010, 2010.

Tokarek, T. W., Huo, J. A., Odame-Ankrah, C. A., Hammoud, D., Taha, Y. M., and Osthoff, H. D.: A gas chromatograph for quantification of peroxycarboxylic nitric anhydrides calibrated by thermal dissociation cavity ring-down spectroscopy, Atmos. Meas. Tech., 7, 3263-3283, 10.5194/amt-7-3263-2014, 2014.

Tokarek, T. W., Brownsey, D. K., Jordan, N., Garner, N. M., Ye, C. Z., Assad, F. V., Peace, A., Schiller, C. L., Mason, R. H., Vingarzan, R., and Osthoff, H. D.: Biogenic emissions and nocturnal ozone depletion events at the Amphitrite Point Observatory on Vancouver Island, Atmosphere-Ocean, 55, 121-132, 10.1080/07055900.2017.1306687, 2017.

Triki, M., Cermak, P., Méjean, G., and Romanini, D.: Cavity-enhanced absorption spectroscopy with a red LED source for NOx trace analysis, Applied Physics B: Lasers and Optics, 91, 195-201, 10.1007/s00340-008-2958-x, 2008.

Varma, R. M., Venables, D. S., Ruth, A. A., Heitmann, U., Schlosser, E., and Dixneuf, S.: Long optical cavities for open-path monitoring of atmospheric trace gases and aerosol extinction, Appl. Optics, 48, B159-B171, 10.1364/AO.48.00B159, 2009.

Vaughan, S., Gherman, T., Ruth, A. A., and Orphal, J.: Incoherent broad-band cavity-enhanced absorption spectroscopy of the marine boundary layer species I_2, IO and OIO, Phys. Chem. Chem. Phys., 10, 4471-4477, 10.1039/b802618a, 2008.

Venables, D. S., Gherman, T., Orphal, J., Wenger, J. C., and Ruth, A. A.: High sensitivity in situ monitoring of NO_3 in an atmospheric simulation chamber using incoherent broadband cavity-enhanced absorption spectroscopy, Environm. Sci. Technol., 40, 6758-6763, 10.1021/es061076j, 2006.

Voigt, S., Orphal, J., and Burrows, J. P.: The temperature and pressure dependence of the absorption cross-sections of NO_2 in the 250-800 nm region measured by Fourier-transform spectroscopy, Journal Of Photochemistry And Photobiology A-Chemistry, 149, 1-7, 10.1016/S1010-6030(01)00650-5, 2002.

Washenfelder, R. A., Langford, A. O., Fuchs, H., and Brown, S. S.: Measurement of glyoxal using an incoherent broadband cavity enhanced absorption spectrometer, Atmos. Chem. Phys., 8, 7779-7793, 10.5194/acp-8-7779-2008, 2008.

Washenfelder, R. A., Flores, J. M., Brock, C. A., Brown, S. S., and Rudich, Y.: Broadband measurements of aerosol extinction in the ultraviolet spectral region, Atmos. Meas. Tech., 6, 861-877, 10.5194/amt-6-861-2013, 2013.

Washenfelder, R. A., Attwood, A. R., Flores, J. M., Zarzana, K. J., Rudich, Y., and Brown, S. S.: Broadband cavity-enhanced absorption spectroscopy in the ultraviolet spectral region for measurements of nitrogen dioxide and formaldehyde, Atmos. Meas. Tech., 9, 41-52, 10.5194/amt-9-41-2016, 2016.

Watson, J., and Estes, J. A.: Stability, resilience, and phase shifts in rocky subtidal communities along the west coast of Vancouver Island, Canada, Ecol. Monogr., 81, 215-239, 10.1890/10-0262.1, 2011.

Werle, P., Mucke, R., and Slemr, F.: The Limits of Signal Averaging in Atmospheric Trace-Gas Monitoring by Tunable Diode-Laser Absorption-Spectroscopy (TDLAS), Applied Physics B-Photophysics and Laser Chemistry, 57, 131-139, 10.1007/BF00425997, 1993.

Wu, T., Zha, Q., Chen, W., Xu, Z., Wang, T., and He, X.: Development and deployment of a cavity enhanced UV-LED spectrometer for measurements of atmospheric HONO and NO_2 in Hong Kong, Atmos. Environm., 95, 544-551, 10.1016/j.atmosenv.2014.07.016, 2014.

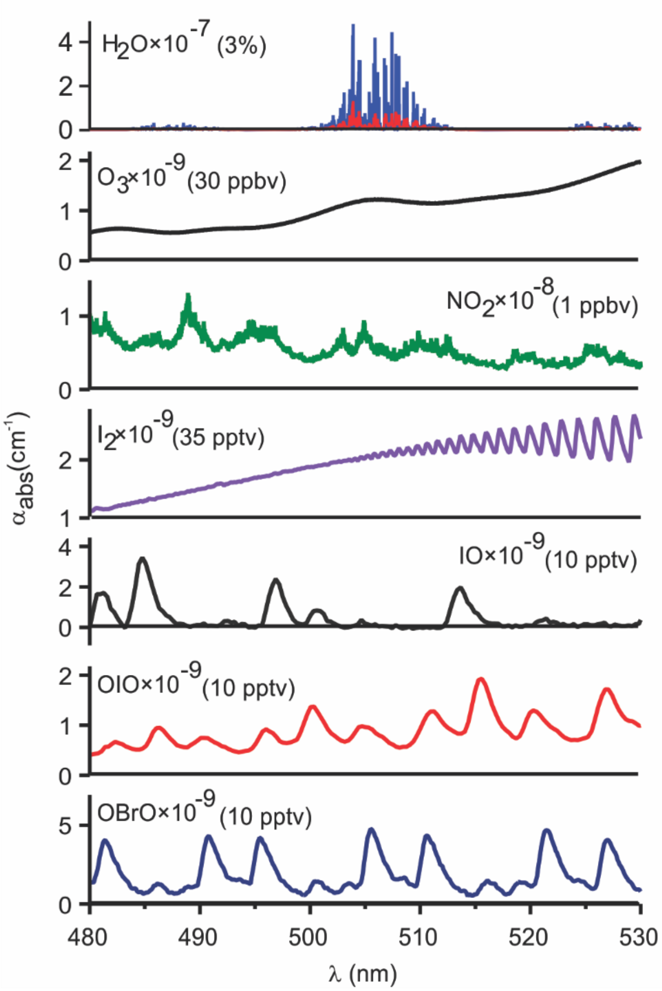

Figure 1. Absorption coefficients for atmospheric absorbers in the cyan region at typical tropospheric ~~abundances~~ mixing ratios (stated in brackets after each species). Absorption cross-sections were downloaded from the Max-Planck Institute for Chemistry's web site located at http://www.uv-vis-spectral-atlas-mainz.org and are based on the following: H_2O (Coheur et al., 2002), O_3 (Burkholder and Talukdar, 1994), NO_2 (Voigt et al., 2002), I_2 (Spietz et al., 2006), IO, OIO (Spietz et al., 2005), and OBrO (Knight et al., 2000). The literature cross-sections for H_2O (shown in blue) were convolved with the resolution of the IBBCEAS (shown in red). The absorption cross-section of O_4 is shown in Figure S4.

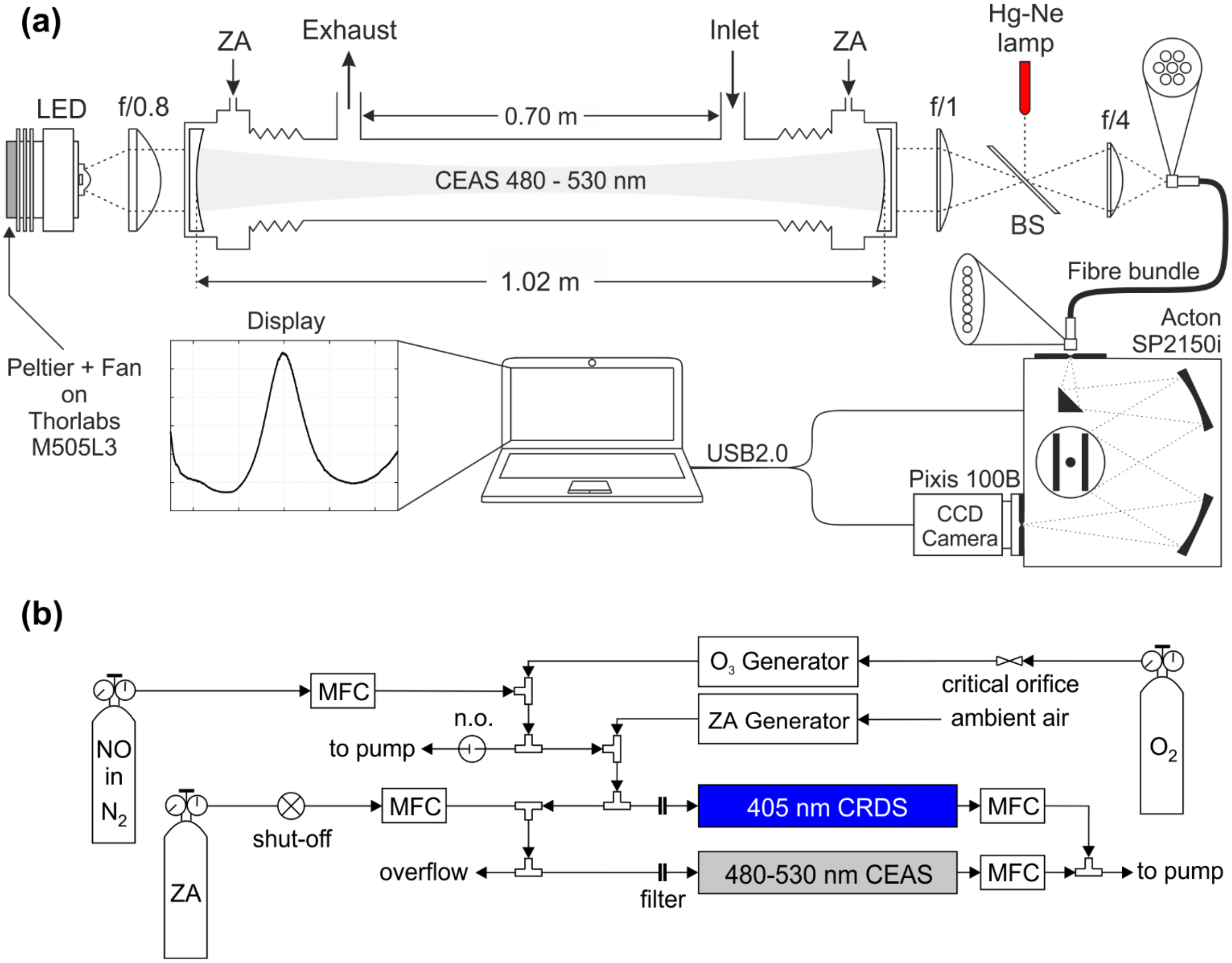

Figure 2. (**a**) Setup of the cyan IBBCEAS (not to scale). (**b**) Setup of NO_2 calibration gas delivery for instrument characterization experiments. Abbreviations: LED – light emitting diode, BS – quartz beam splitter, CCD – charge-coupled device, ZA – zero air, USB – universal serial bus, and MFC – mass flow controller.

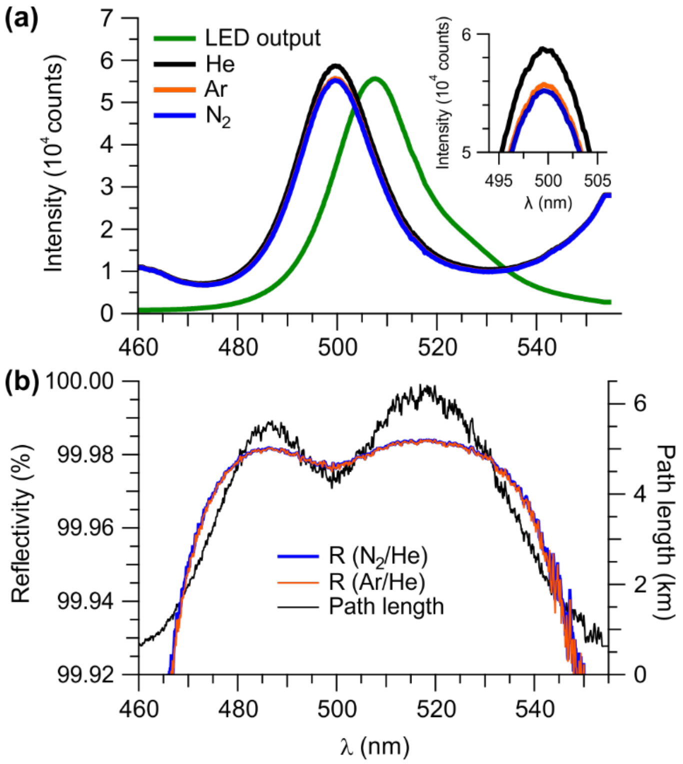

Figure 3. (**a):** Transmission spectra (averaged over 15 min) observed when the sample cell was filled with He, Ar, or N_2 at ambient pressure (890 hPa)~~.~~ The LED output spectrum (in arbitrarily scaled units) is superimposed. (**b):** Mirror reflectivity and effective path length (based on Ar/He) calculated from the data shown in panel (a).

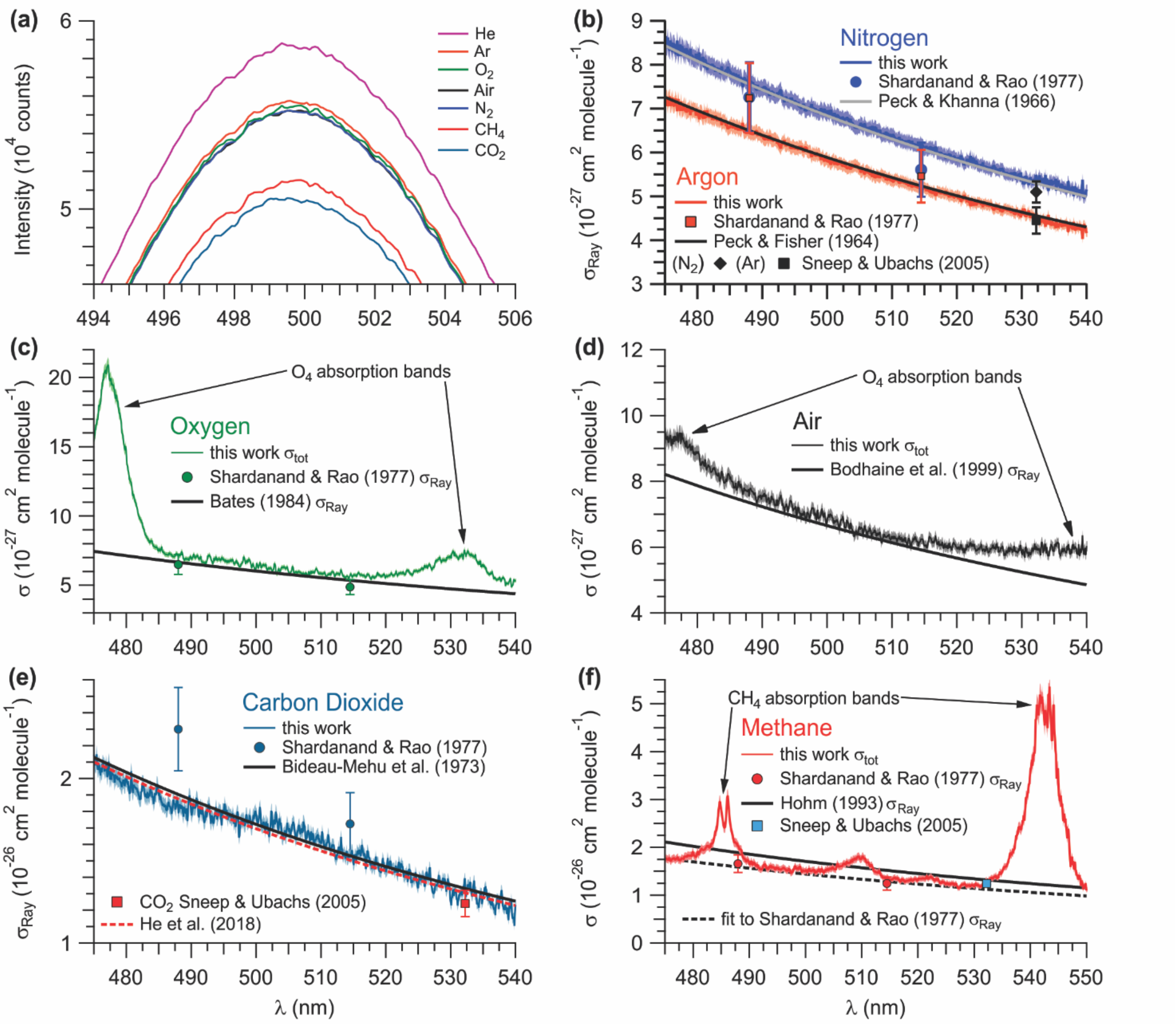

Figure 4. Measurements of pure gases. **(a)** Relative intensities of the IBBCEAS signal due to each sampled gas. Extinction cross-sections of **(b)** 99.998% N_2 (shown in blue) and 99.998% Ar (red), **(c)** air (black), **(d)** 99.99% O_2 (green), **(e)** 99.95% CO_2 (teal), and **(f)** 99.97% CH_4 (red). Shaded areas represent ±2.5% error margin in N_2, Ar, O_2, air, and CO_2, and 4.6% in CH_4. σ_{Ray} - Rayleigh scattering cross-section; σ_{tot} = total extinction cross-section ($=\sigma_{Ray} + \sigma_{abs}$).

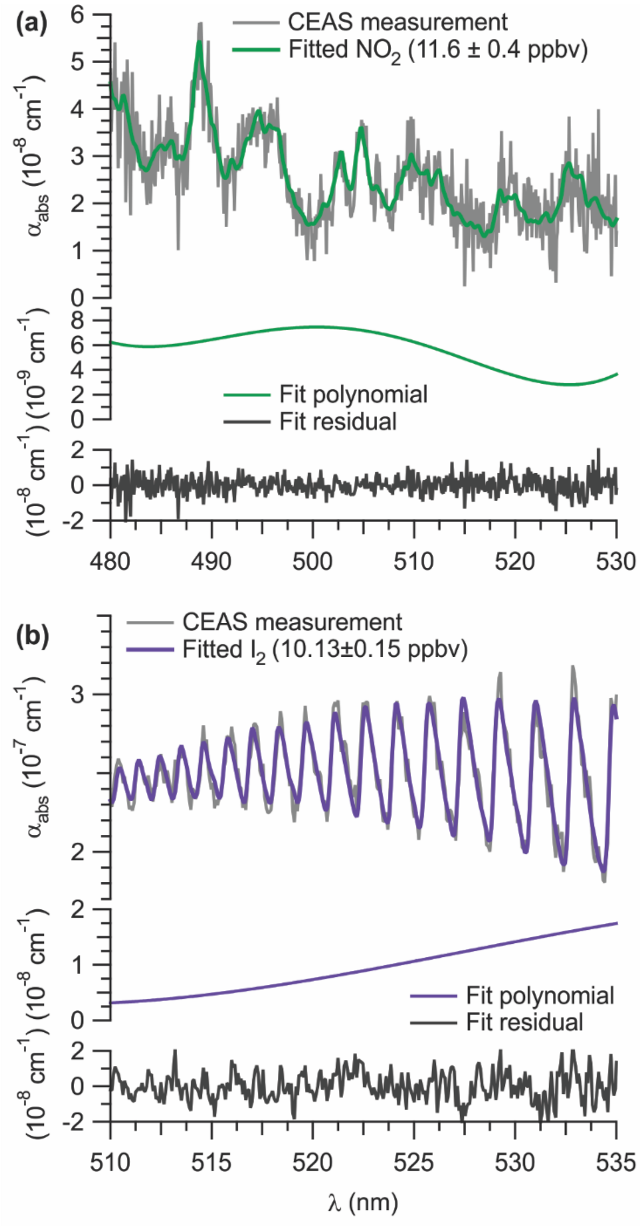

Figure 5. Spectral fits to 60 s IBBCEAS signal, including a 3rd order polynomial and fit residual, for **a)** NO_2 (ambient) and **b)** I_2 (calibration) during the ORCA field campaign.

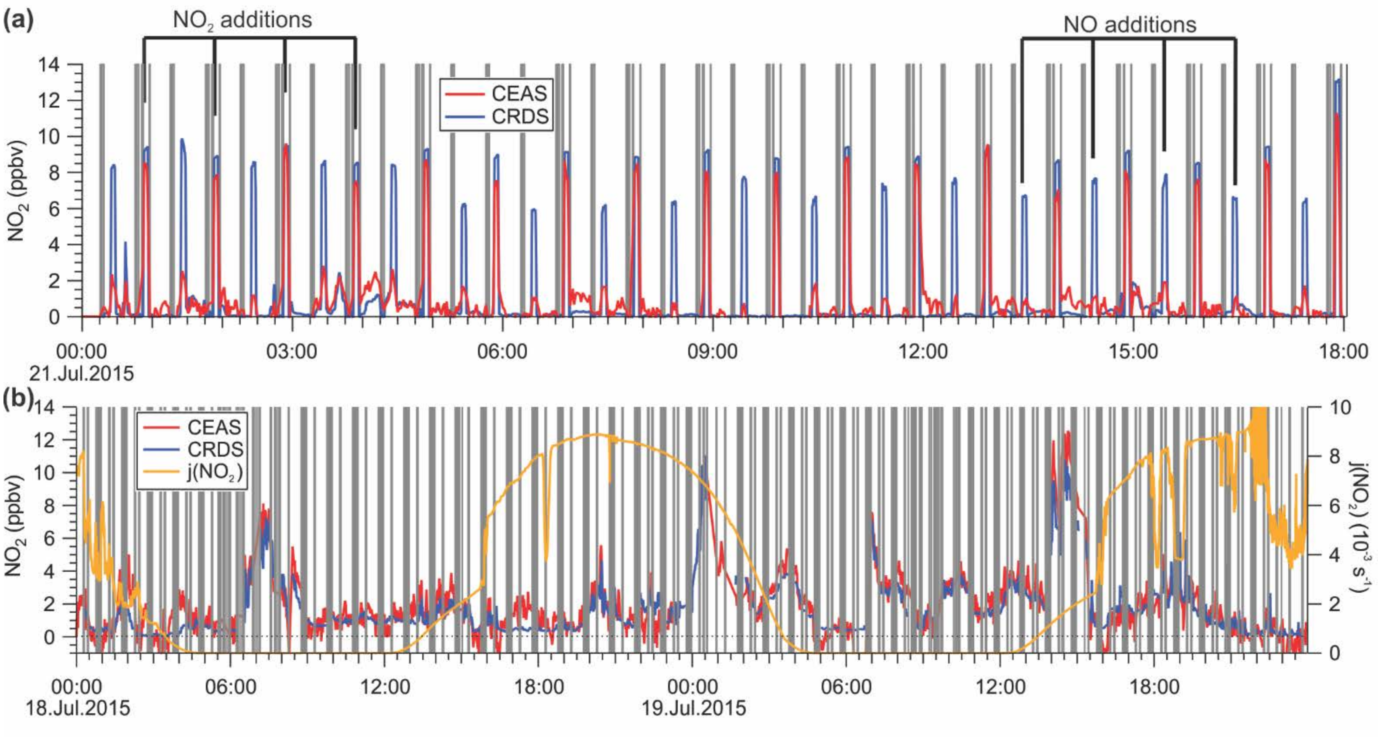

Figure 6. (a) Sample time series of continuous IBBCEAS and CRDS data collected during the ORCA campaign showing measurements of ambient air, NO_2-free "zero" air (every 30 min), and hourly standard additions of NO_2 (~10 ppbv) in "zero air" and NO (~130 ppbv) to ambient air. The areas shaded in grey indicate times when both instruments sampled zero air. When high concentrations of NO were added, more NO_2 was observed by CRDS due to this instrument's longer inlet residence time. (**b**) Sample time series of ambient air NO_2 mixing ratios observed by IBBCEAS and CRDS during ORCA.

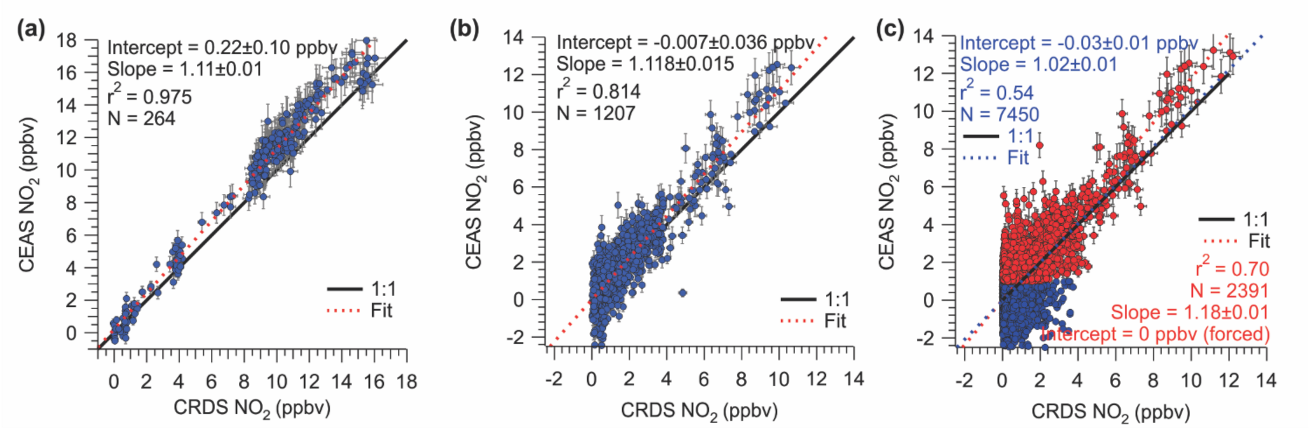

Figure 7. Scatter plots and straight-line fits of IBBCEAS and CRDS NO_2 mixing ratios for: **(a)** standard additions and calibrations, **(b)** ambient air measurements on 18-19 Jul~~,~~ 2015, and **(c)** ambient air measurements of the entire campaign. For the fit line shown in red, IBBCEAS retrievals with NO_2 mixing ratios <1 ppbv were excluded. All data were averaged to 60 s.

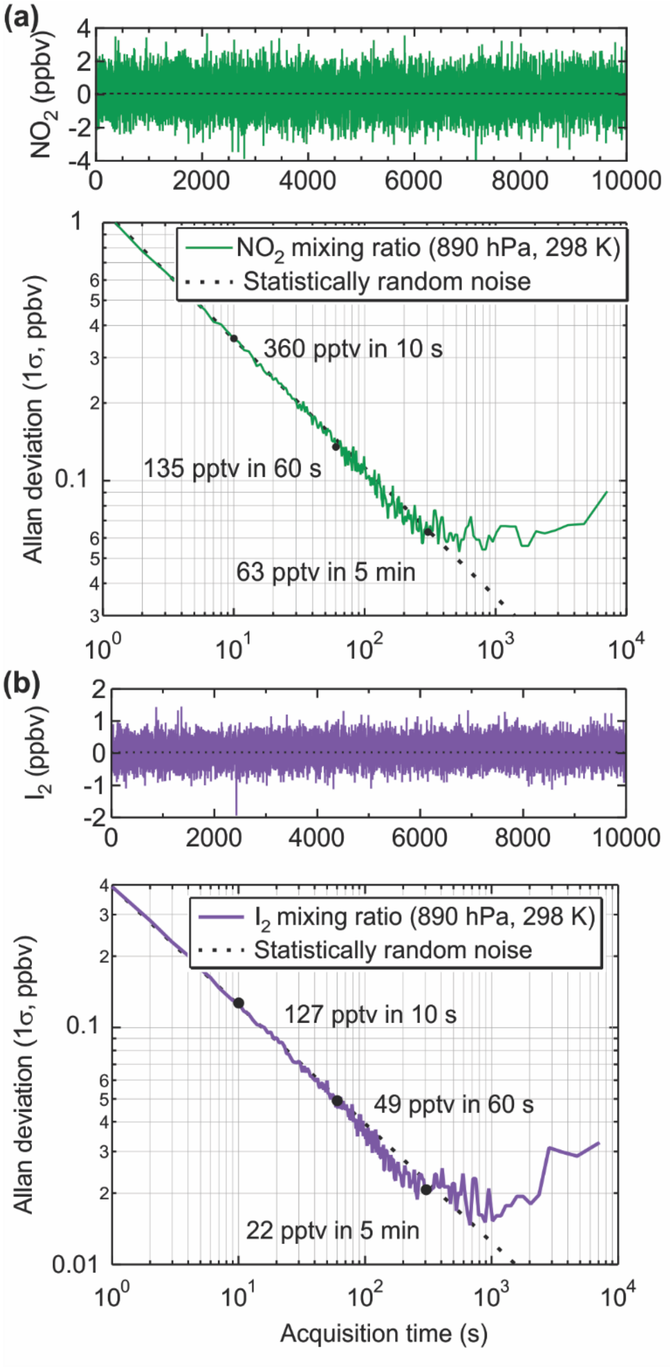

Figure 8. Allan deviation plots of data collected while the IBBCEAS was sampling zero air to determine the optimum integration time of: (**a**) the calculated NO_2 mixing ratios at ~~668 Torr~~890 hPa (1.5 slpm sample rate) and 298 K, and

810 (**b**) the calculated I_2 mixing ratios under the same conditions.

Table 1. Summary of observed and *n*-based Rayleigh scattering cross-sections.

Gas (Purity)	λ (nm)	σ_{Ray} (this work)[a] (10^{-27} cm^2 molecule^{-1})	σ_{Ray} (*n*-based)[b] (10^{-27} cm^2 molecule^{-1})	σ_{Ray} (CRDS)[d] (10^{-27} cm^2 molecule^{-1})	$(n\text{-}1)$ $\times 10^{-6}$	F_k[c]
N_2 (99.998%)	485.03	7.85	7.74	-	284.97	1.034
	495.08	7.16	7.12	-	284.70	
	505.01	6.61	6.56	-	284.45	
	515.06	6.09	6.06	-	284.22	
	525.07	5.61	5.60	-	283.99	
	532.20	5.49	5.30	5.1(±0.2)	283.84	
O_2 (99.99%)	485.03	-	6.83	-	273.34	1.096
	495.08	6.84	6.28	-	273.03	
	505.01	5.96	5.78	-	272.74	
	515.06	5.72	5.33	-	272.46	
	525.07	-	4.93	-	272.21	
Air[e]	485.03	-	7.54	-	279.38	1.133
	495.08	7.22	6.93	-	279.10	
	505.01	6.60	6.39	-	278.84	
	515.06	6.04	5.89	-	278.59	
	525.07	-	5.45	-	278.36	
Ar (99.998%)	485.03	6.58	6.67	-	269.02	1.000
	495.08	6.10	6.13	-	268.77	
	505.01	5.61	5.65	-	268.54	
	515.06	5.19	5.22	-	268.31	
	525.07	4.81	4.82	-	268.11	
	532.20	4.40	4.56	4.4 (±0.3)	267.97	
CO_2 (99.97%)	485.03	19.0	19.5	-	429.81	1.136
	495.08	18.0	17.9	-	429.33	
	505.01	16.9	16.5	-	428.88	
	515.06	14.7	15.2	-	428.46	
	525.07	13.7	14.1	-	428.06	
	532.20	13.9	13.3	12.4(±0.8)	427.79	
CH_4 (99.95%)	492.06	15.4	15.4[f]	-	483.22	1.000
	497.46	14.7	14.7[f]	-	482.87	
	501.72	14.5	14.2[f]	-	482.59	
	516.92	12.8	12.6[f]	-	481.66	
	527.28	11.6	11.7[f]	-	481.08	
	532.20	13.1	13.2[f]	12.5(±0.2)	480.81	

[a] The absolute uncertainty is ±2.5% (see Sect. 4.1); [b,c] See text for references of *n*-based scattering cross-sections and references therein for corresponding calculations of King (King, 1923) correction factors; [d] From (Sneep and Ubachs,

2005); uncertainty is stated as 1σ. [e] The ratio of N_2/O_2 in the cylinder was ~ 80.5/19.5; [f] Comparison is to the fitted expression to the data set of (Shardanand and Rao, 1977).

Table 2. Selected CEAS detectors for quantification of NO_2 in the near-UV and visible region of the electromagnetic spectrum

	Arc 330 (Washenfelder et al., 2016)	Violet 365 (Gherman et al., 2008)	Blue 455 (Min et al., 2016)	Blue 455 (Langridge et al., 2006)	Blue 465 (Thalman and Volkamer, 2010)	Red 643 (Triki et al., 2008)	Red 660 (Wu et al., 2014)	Cyan 508 (This work)
Light source manu-facturer	Energetiq	Omicron Latronics	LEDEngin	Lumileds Luxeon	LEDEngin	Lumileds Luxeon	Marubeni America	Thorlabs
model	Laser-driven arc lamp	n/a	LZ1-00DB05	LXHL–PR09	LZ1–00DB05	LXHL–MD1D	SMB660N-1100	M505L3
optical power (W)	125 W	0.105	1	0.450	1.0	0.190	0.300	0.440
λ_p±FWHM[a] (nm)	n/a	365±12	460±5	455±20	465±22	643±20	660±14	508±30
Fit range(s) (nm)	315-350	366 – 378	438 – 468	441 – 463	435 – 465 455 – 487	640 – 670	353 – 376	480 – 530
Mirror reflectivity (%)	99.93	99.94	99.997	99.976	99.9964	99.991	99.925	99.9998
Cell length (m)	1.00	1.15 and 4.50	0.48	1.50	0.99	2.00	1.76	1.02
Path length[b] (km)	1.43	1.9 and 7.5	17.8	6.25	27.5	22	2.1	510
Integration time (s)	30	600	5	30	60	60	120	60
LOD (1σ, ppbv)	0.14#	0.38*	0.04#	0.10*	0.030	9.0*	1	~~0.11~~0.14* 0.53#

[a] peak wavelength + full-width at half maximum; [b] effective path length, L_{eff} = 1/(1-R); * laboratory sample; # field samples

Supplementary Figures for:

A broadband cavity-enhanced spectrometer for atmospheric trace gas measurements and Rayleigh scattering cross sections in the cyan region (470-540 nm)

Nick Jordan[1], Connie Z. Ye,[1] Satyaki Ghosh,[1] Rebecca Washenfelder,[2] Steven S. Brown,[2] and Hans D. Osthoff[1]

[1]Department of Chemistry, University of Calgary, 2500 University Drive NW, Calgary, AB T2N 1N4, Canada

[2]Earth System Research Laboratory, National Oceanic and Atmospheric Administration, Boulder, CO 80303, USA

Correspondence: Hans D. Osthoff (hosthoff@ucalgary.ca)

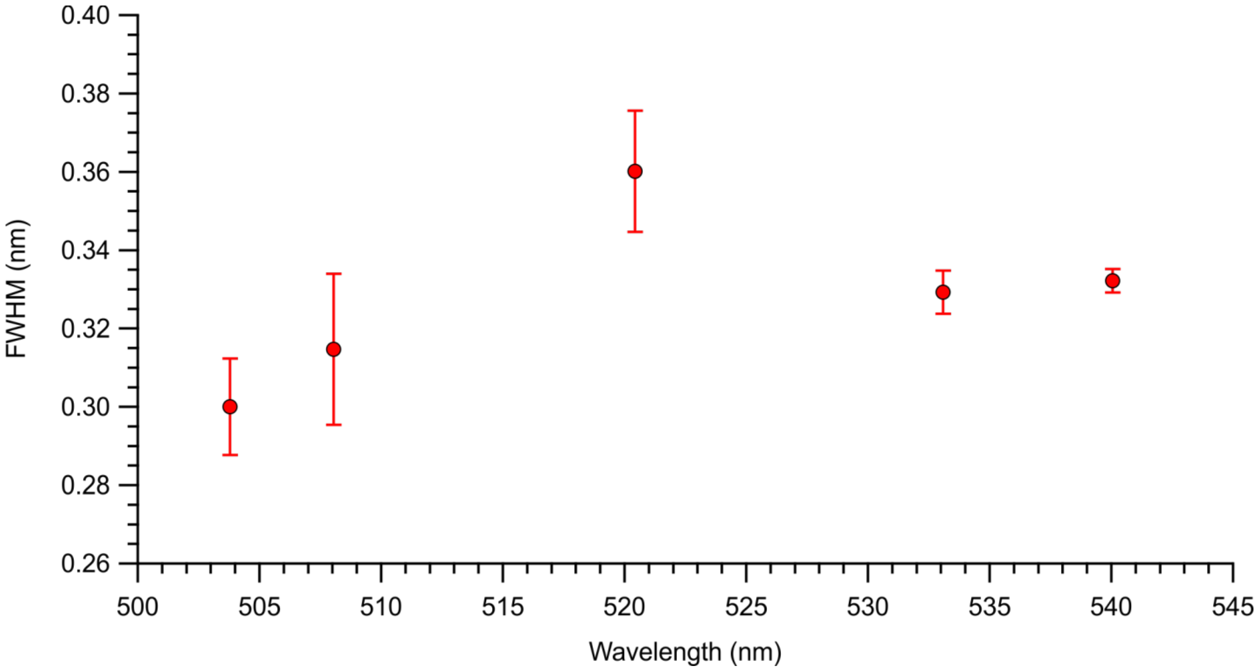

Figure S1 Full width half maximum (FWHM = 2 × width × $(\ln(2))^{1/2}$) values calculated for sharp peaks in the Hg(Ne) calibration source and 50 µm spectrometer slit width. The error bars represent 1σ of the Gaussian peak fitted to each line in the lamp spectrum.

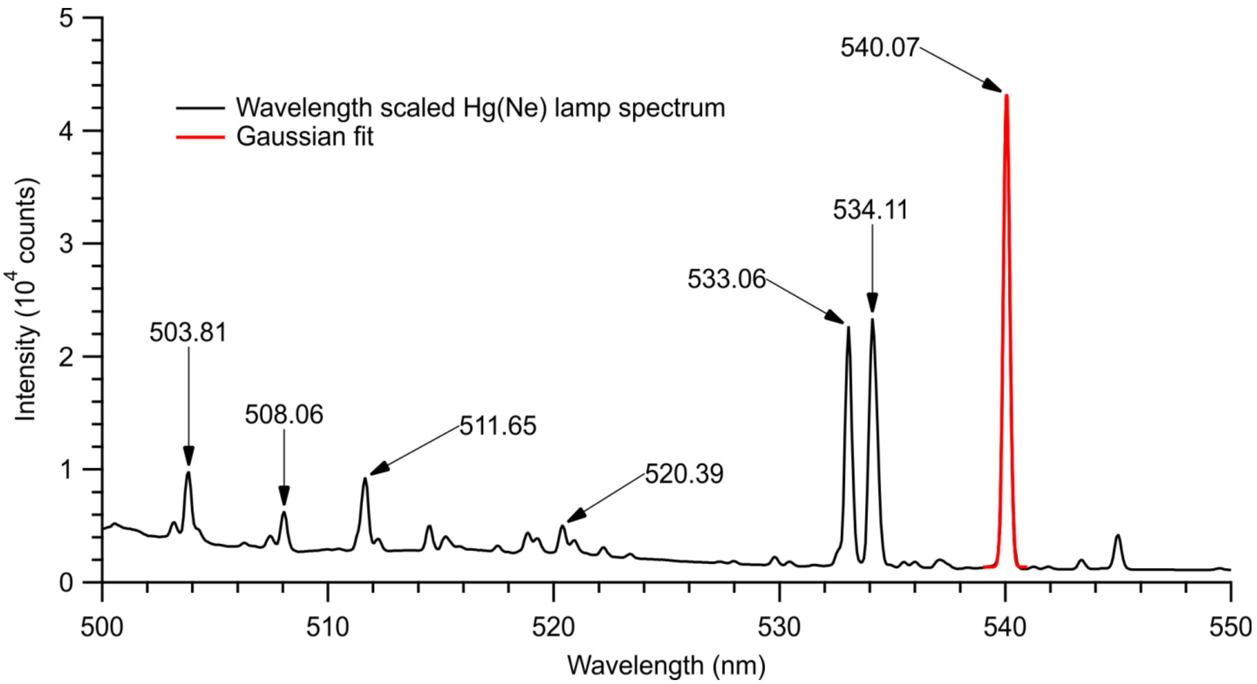

Figure S2 Wavelength calibrated Hg(Ne) lamp spectrum recorded using Acton SP2156 spectrograph equipped with PIXIS 100B CCD camera. The spectrum was produced by the average of 120 one second scans.

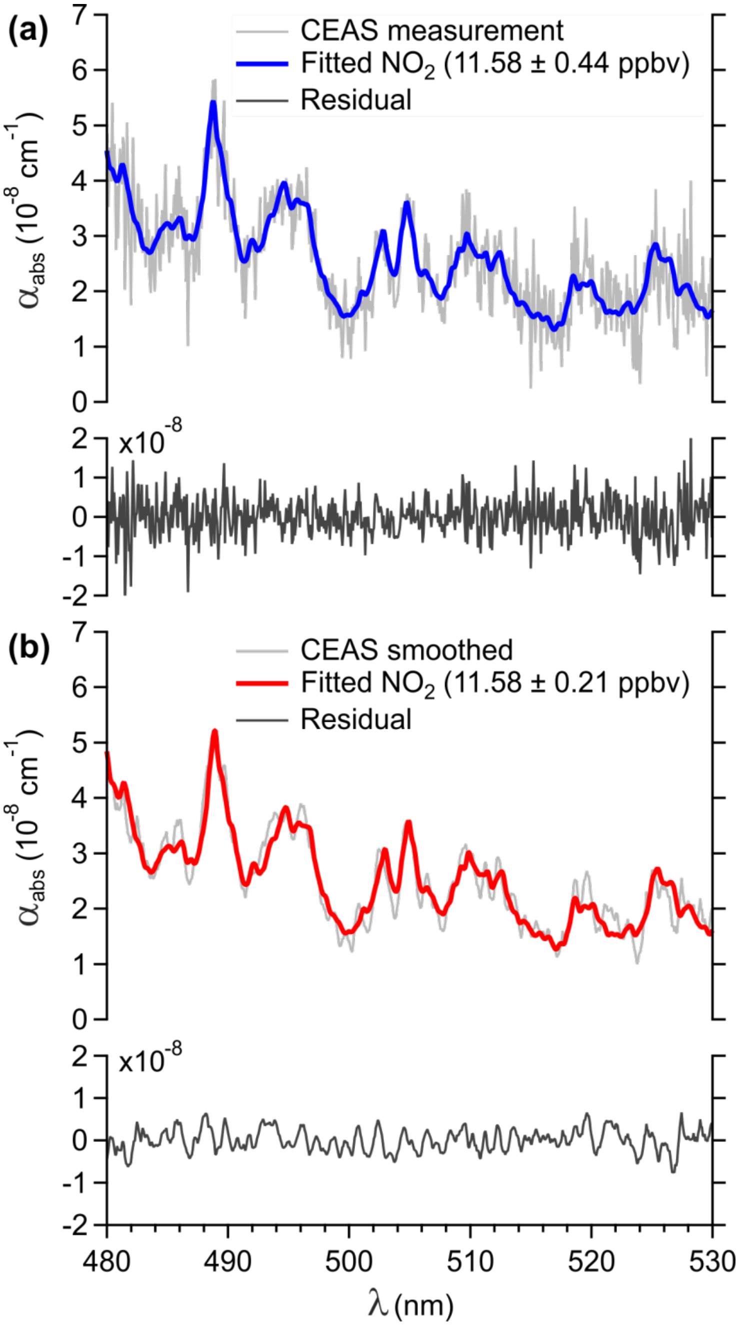

Figure S3 Example of fitted spectra for **a)** NO_2 without smoothing and **b)** NO_2 with smoothing using a fourth degree polynomial Savitzky-Golay (1964) filter.

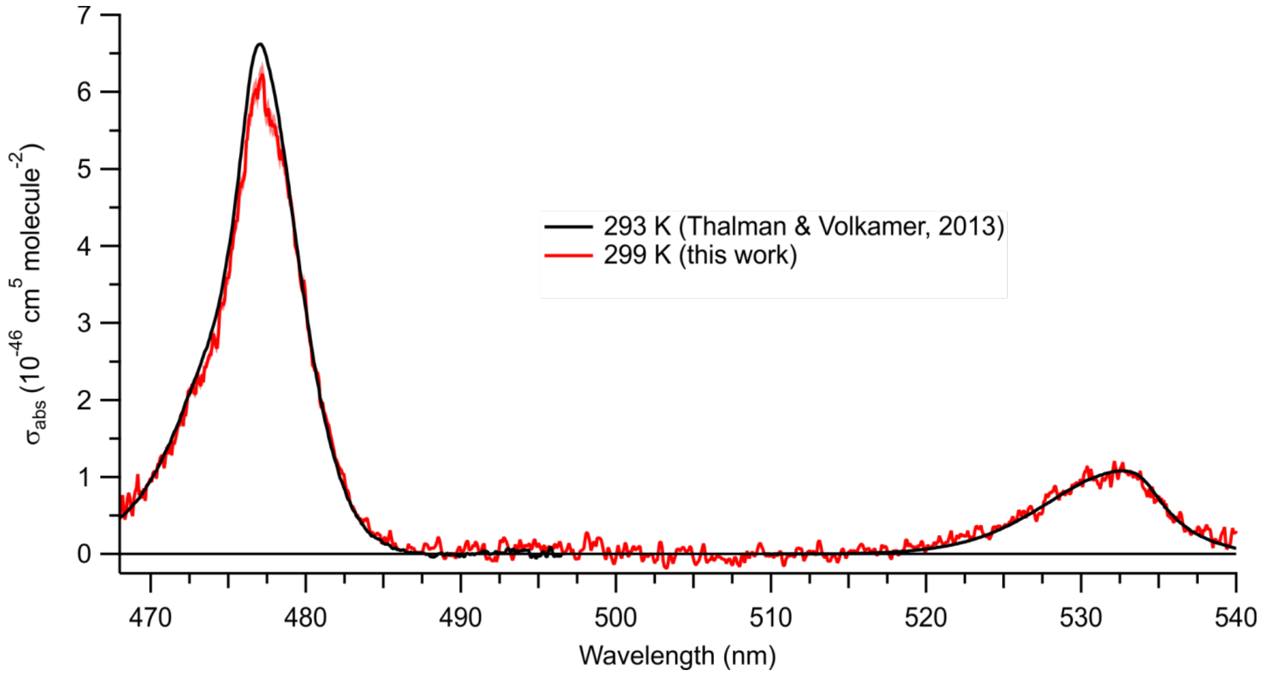

Figure S4 Room-temperature absorption cross-section of O_4, calculated from the data shown in Figure 4c. Data from (Thalman and Volkamer, 2013) are superimposed.

Table S1. Selected absorption cross-sections of O_4 at room temperature in the recent literature.

Reference	**Peak σ(477 nm)** (10^{-46} cm^5 $molecule^{-2}$)	**Peak σ(532 nm)** (10^{-46} cm^5 $molecule^{-2}$)
~~Greenblatt, 1990~~ (Greenblatt et al., 1990)	6.3±0.6	1.0±0.1
~~Newnham and Ballard, 1998 @283K~~ (Newnham and Ballard, 1998)	8.3±0.8	1.2±0.4
~~Hermans et al., 1999~~ (Hermans et al., 1999)	6.6	1.1
~~Sneep and Ubachs, 2005~~ (Sneep and Ubachs, 2005)	-	1.01±0.03
~~Sneep et al., 2006~~ (Sneep et al., 2006)	6.60±0.06	-
~~Thalman and Volkamer, 2013~~ (Thalman and Volkamer, 2013)	6.6±0.1	1.09±0.06
This work	6.2±0.5	1.08±0.09

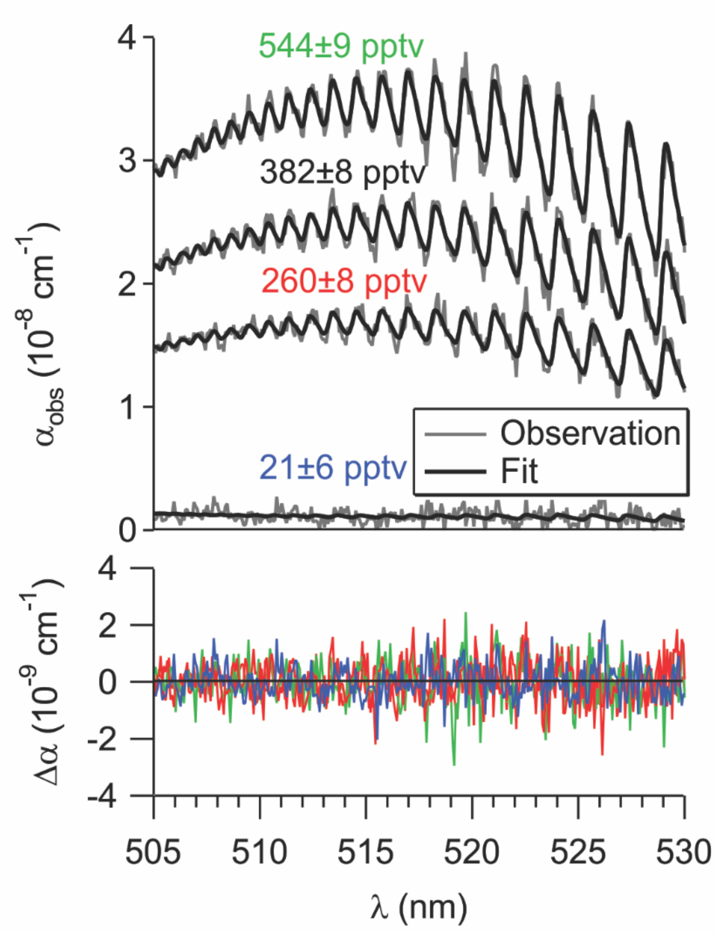

Figure S5 Examples of ~~S~~spectral fits of laboratory generated I_2 at different mixing ratios.~~.~~ The absorption cross-sections by Spietz et al. (2006) and a third-order polynomial were used. The bottom panel shows the fit residuals, colour-coded by the mixing ratio labels above.

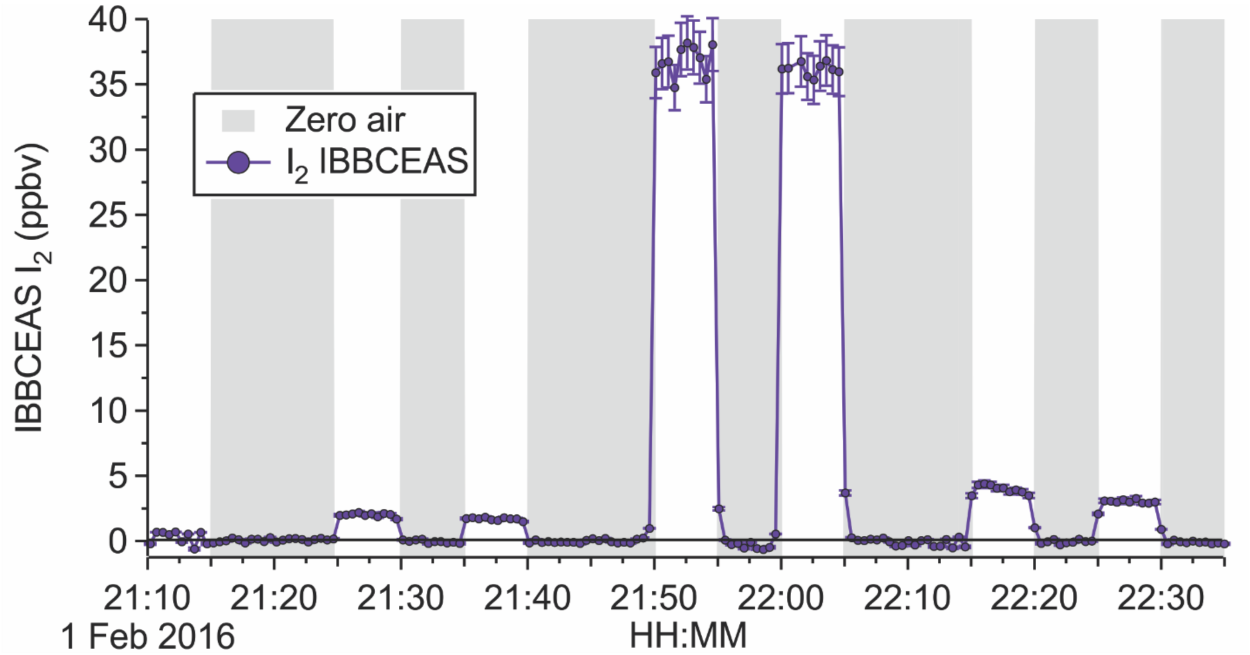

Figure S6 Time series of sample CEAS retrievals while sampling laboratory generated I_2. The grey underlay indicates times when the instrument sampled zero air. Iodine was delivered from four permeation tubes of different wall thickness, which were exchanged during the zeroing periods while the diffusion chamber output was bypassed.

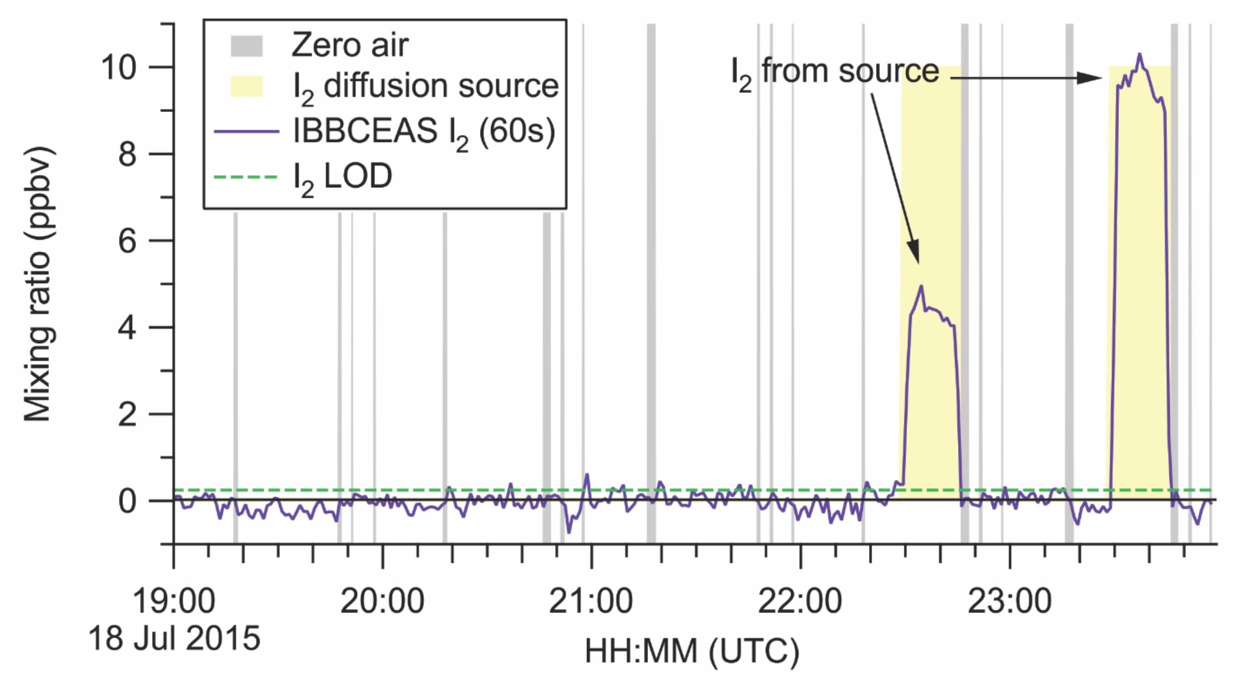

Figure S7 Time series of ambient air I_2 measurements during the ORCA campaign. The green dashed line represents the 2σ LOD for I_2. The grey shaded areas indicate periods when the CEAS sampled zero air. The yellow shaded areas indicate times when the CEAS sampled I_2 from a permeation which was controlled to a temperature of 40 °C at 22:30 and 55 °C at 23:30 UTC.

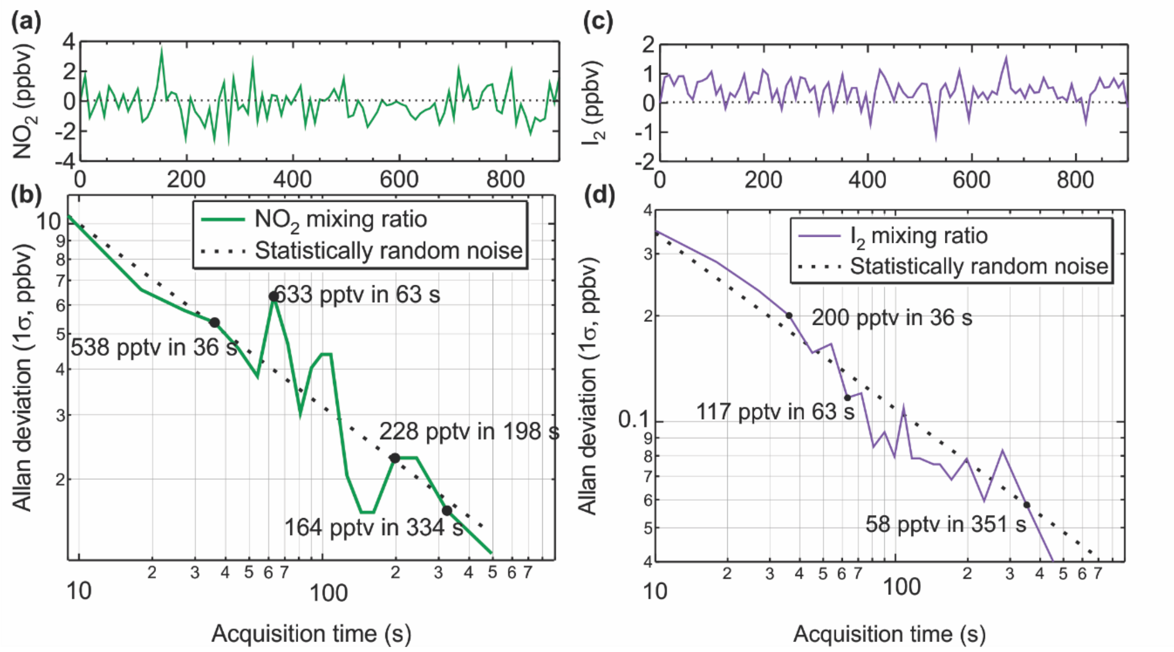

Figure S8 ~~Allan deviation plots of Allan deviation plots of d~~Data collected while the CEAS ~~was sampling~~continuously sampled zero air during the ORCA campaign at a sample cell pressure of 467 hPa, flow rate of 5 slpm, and at a temperature 290 K. (**a**) Time series of NO$_2$ mixing ratios. ~~to determine the optimum integration time of:~~(**b**) Allan deviation plot of the above data. (**c**) Time series of I$_2$ mixing ratios. (**d**) Allan deviation plot of the above data. ~~**(a)** a single pixel at 500 nm in the lab at 668 Torr (1.5 slpm sample rate) and 298 K, and **(b)** NO$_2$ mixing ratios during the ORCA campaign at 350 Torr (5 slpm sample rate) and 290 K.~~

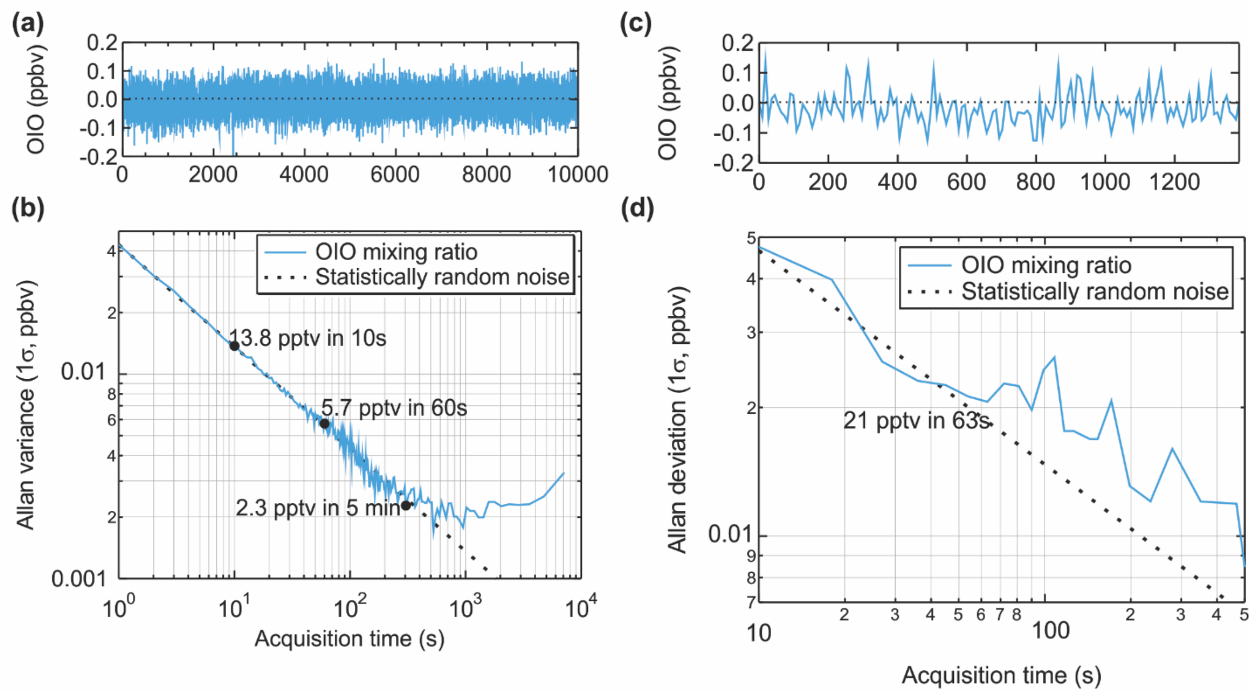

Figure S9 (left hand side) Data collected while the CEAS continuously sampled zero air in the laboratory at a sample cell pressure of 890 hPa, flow rate of 1.5 slpm, and at a temperature 298 K. (**a**) Time series of OIO mixing ratios. (**b**) Allan deviation plot of the above data. (right hand side) Data collected while the CEAS continuously sampled zero air during the ORCA campaign at a sample cell pressure of 467 hPa, flow rate of 5 slpm, and at a temperature 290 K. (**c**) Time series of OIO mixing ratios during ORCA. (**d**) Allan deviation plot of the above data.

~~Allan deviation plots of data collected while the CEAS was sampling zero air to determine the optimum integration time and detection limits of: (**top**) I_2 during ambient sampling conditions; (**bottom left**) the calculated OIO mixing ratios in the lab at 668 Torr (1.5 slpm sample rate) and 298 K, and (**bottom right**) OIO mixing ratios during the ORCA campaign at 350 Torr (5 slpm sample rate) and 290 K.~~

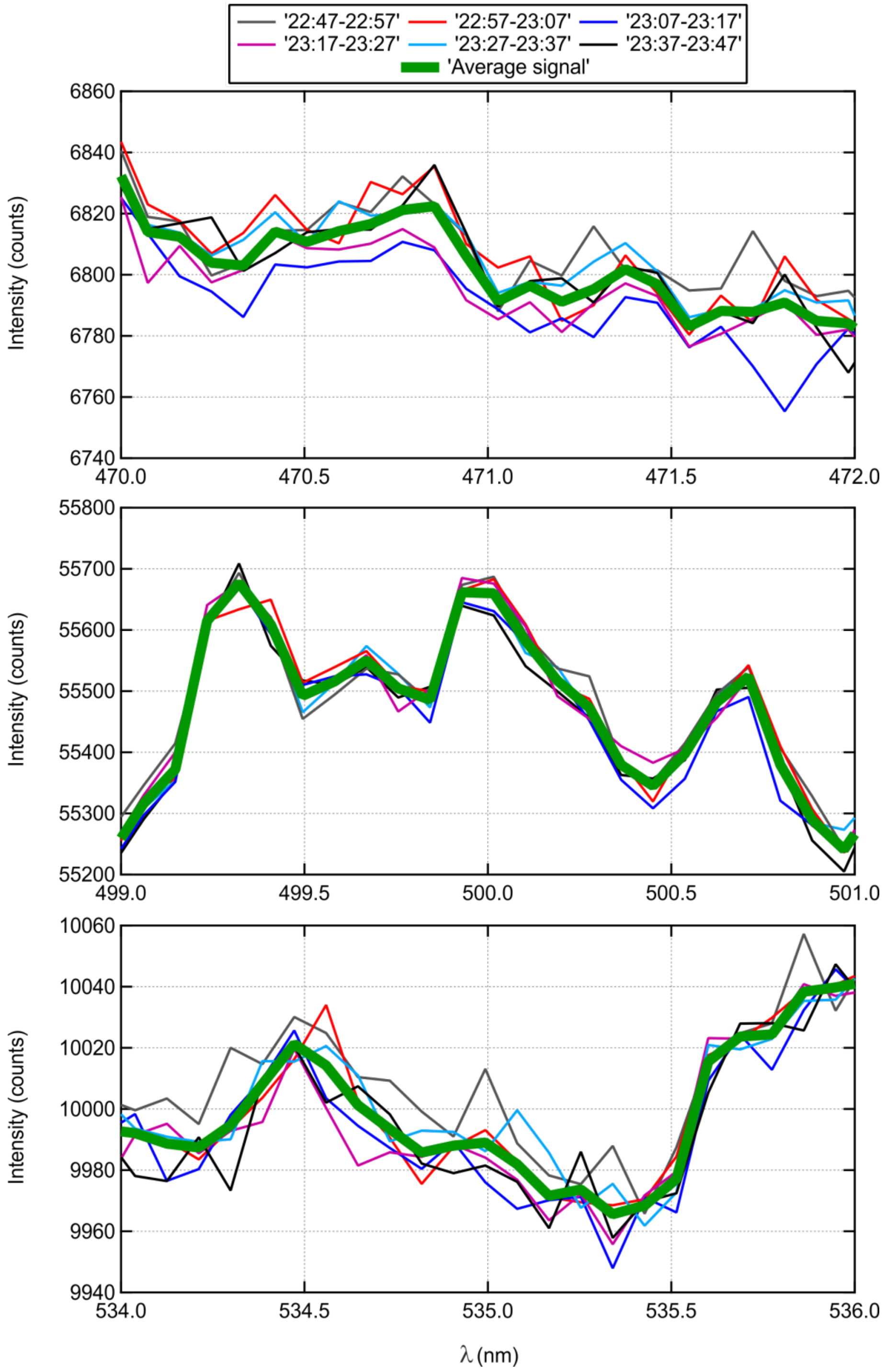

Figure S10 ~~CEAS emission profile for~~Intensity of light exiting a a cavity filled with zero air. Three different wavelength regions within the emission spectrum of ~~and~~ the~~a~~ LED (M505L3) ~~driven~~ operated at 30.0±0.1 °C are shown. The stability of the emission profile was monitored over a 60 min interval with a LED warm up time of 30 min prior to measurements. Each trace represents a 10 min average while the thick green trace shows 60 min average.

References

Greenblatt, G. D., Orlando, J. J., Burkholder, J. B., and Ravishankara, A. R.: Absorption Measurements of Oxygen Between 330 and 1140 nm, J. Geophys. Res., 95, 18577–18582, 10.1029/JD095iD11p18577, 1990.

Hermans, C., Vandaele, A. C., Carleer, M., Fally, S., Colin, R., Jenouvrier, A., Coquart, B., and Mérienne, M.-F.: Absorption cross-sections of atmospheric constituents: NO_2, O_2, and H_2O, Environm. Sci. Poll. Res., 6, 151-158, 10.1007/bf02987620, 1999.

Newnham, D. A., and Ballard, J.: Visible absorption cross sections and integrated absorption intensities of molecular oxygen (O_2 and O_4), J. Geophys. Res.-Atmos., 103, 28801-28815, 10.1029/98JD02799, 1998.

Savitzky, A., and Golay, M. J. E.: Smoothing and Differentiation of Data by Simplified Least Squares Procedures, Anal. Chem., 36, 1627-1639, 10.1021/ac60214a047, 1964.

Sneep, M., and Ubachs, W.: Direct measurement of the Rayleigh scattering cross section in various gases, J. Quant. Spectrosc. Radiat. Transfer, 92, 293-310, 10.1016/j.jqsrt.2004.07.025, 2005.

Sneep, M., Ityaksov, D., Aben, I., Linnartz, H., and Ubachs, W.: Temperature-dependent cross sections of O_2-O_2 collision-induced absorption resonances at 477 and 577 nm, J. Quant. Spectrosc. Radiat. Transf., 98, 405-424, 10.1016/j.jqsrt.2005.06.004, 2006.

Spietz, P., Gómez Martín, J., and Burrows, J. P.: Effects of column density on I_2 spectroscopy and a determination of I_2 absorption cross section at 500 nm, Atmos. Chem. Phys., 6, 2177-2191, 10.5194/acp-6-2177-2006, 2006.

Thalman, R., and Volkamer, R.: Temperature dependent absorption cross-sections of O_2-O_2 collision pairs between 340 and 630 nm and at atmospherically relevant pressure, Physical Chemistry Chemical Physics, 15, 15371-15381, 10.1039/c3cp50968k, 2013.